"The idea is to try to give all the information to help others to judge the value of your contribution; not just the information that leads to judgment in one particular direction or another."

~

Richard Philips Feynman

University of Alberta

High Speed Paraffin Nanocomposite Phase Change Microactuator for
Microvalve Applications

by

Samira Movahedian

A thesis submitted to the Faculty of Graduate Studies and Research
in partial fulfillment of the requirements for the degree of

Master of Science

in

Mircosystems and Nanodevices

Department of Electrical and Computer Engineering

© Samira Movahedian
Fall 2012
Edmonton, Alberta

For my parents.

Thank you for your love and encouragements.

Abstract

Microvalves are an essential part of microfluidic systems for chemical and biological analysis. However, the lack of high performance materials has hindered the development of microactuators capable of driving valves with combined rapid response and high closing forces. Paraffin-based phase change microvalves achieve high open/close flow ratios and closing pressures, which minimize leakage. In addition, they are stable and easy to fabricate. However, these valves are intrinsically slow, due to the low thermal conductivity of paraffin coupled to its high specific heat capacity. We report on a rapid response phase change microactuator for microvalve applications based on a polymer membrane and a novel composite of paraffin and high thermal conductivity nanoparticles. By modifying the thermal properties of paraffin, faster heat transfer and actuation speed can be achieved. This design can be used to fabricate microvalves in contamination-sensitive lab-on-chip (LOC) systems where low leakage and high speed flow control are required.

Acknowledgments

I would like to thank my great supervisors Dr. Thomas Thundat and Dr. Stephane Evoy for accepting me as their student and for their patient guidance and advice throughout my graduate study. Thanks for supporting me all the time and for giving me lots of self-confidence. I have been amazingly fortunate to have advisors who gave me freedom to explore my research, and I'm so proud to be your student. Special thanks to Dr. Zubin Jacob, Dr. Neda Nazemifard for accepting to be in my examination committee.

I'm grateful to Dr. Sameoto for his guidance and practical advice. I am also thankful to him for helping me to improve my knowledge in the area.

I would like to thank all the staff at the Nanofab for providing training and support through my research. Many thanks to my great colleague Jose Martinez-Quijada, who helped me a lot in designing and testing of the system. I would also like to acknowledge Dave Hedden for his valuable guidance during this work.

I would also like to thank Mohammad Khalkhali, Garima Thakur, Prashanthi Kumar, Mohammad Behnam and Eric Hawk for being such great friends. Their friendship has made my graduate life a unique and one of the greatest experiences in my life. I will never ever forget their endless helps during various stages of my project.

Finally, I would like to express my heartfelt thanks to my wonderful parents for their continued and unconditional support and encouragement along my journey of graduate study. Thanks for being a constant and active presence in my life and for giving me freedom to pursue my dreams. Mama you were always by my side when I was frustrated. You were always the person who I looked up to and you have been a great hero in my life, my greatest strength.

Table of contents

List of Tables

List of Figures

List of Symbols

°C	degree Celsius
ε_0	permittivity of free space
ε_r	dielectric permittivity of the plates
μ	micro
ν	Poisson's ratio
A	surface area
Au	gold
C	capacitance
CE	capillary electrophoresis
cm	centimeter
Cr	chromium
d	distance
D	flexural rigidity of the membrane
DSC	differential scanning calorimetry
DNA	deoxyribonucleic acid
E	Young's modulus
F	force
g	grams
GBL	gamma-Butyrolactone
GPa	gigapascal
h	thickness of the membrane
I	current
IC	integrated circuit
in.Hg	inches of mercury
IPA	isopropyl alcohol
LOC	lab-on-chip
K	kilo
Kg	kilogram

KN	kilonewton
KPa	kilopascal
m	meter
MEMS	micro-electro-mechanical systems
mg	milligram
mW	milliwatt
nl	nanoliter
nm	nanometer
NPs	nanoparticles
p	pressure
PC	phase change
PCR	polymerase chain reaction
PDMS	polydimethylsiloxane
PEB	post exposure bake
PETG	polyethyleneterephthalateglycol
PMMA	polymethylmethacrylate
r	radial distance
rpm	revolutions per minute
s	second
SEM	scanning electron microscope
TEM	transmission electron microscopy
UV	ultraviolet
V	volts
VLSI	very large scale integration
ω	displacement of the membrane

Chapter 1

Introduction

Microfluidics is the enabling technology of future lab-on-chip (LOC) systems for chemical and biological analysis in applications such as medical diagnosis and pollutant detection. Microfluidics offers great advances over conventional macro-scale analytical devices such as use of small sample/reagent volumes, portability and faster analysis time [1]. As a consequence of these advantages, there has been a growing interest in the development of miniaturized microfluidic systems for integrated, portable and accessible diagnostic devices [3].

Microfluidic systems normally consist of an array of interconnected fluidic channels with diameters ranging between 10 to 1000 μm [3]. Efficient flow control in these systems is fundamental, and hence microvalves are the key elements and one of the most important building blocks behind this technology [4]. Microvalves can control the fluid flow within microfluidic system by sealing sections on the microchip. They have been classified in the form of active and passive microvalves employing mechanical, non-mechanical and external systems [5]. Active microvalves demand a microactuator powered by an external source and have a complicated fabrication process. However, passive microvalves are microvalves without actuators [6], they are easy to fabricate and have simple structures. They show diode-like characteristic and only open to forward pressure

[7]. There are various kinds of microactuators that can be used in active microvalve systems such as piezoelectric [8], electostatic [9], electrochemical [10], phase-change [11], shape memory alloy [12], and pneumatic [13].

Despite significant advancements in the field of microfluidics, there are still limitations such as bulky and expensive supporting equipment of microvalves that make it difficult to integrate them into a single portable device [14], [15].

We present a rapid response phase change (PC) polymer microactuator for microvalve application in LOC systems comprised of a reservoir sealed by a flexible membrane and filled with a phase change nanocomposite. Such a composite consists of paraffin loaded with gold (Au) nanoparticles, which provide a high thermal conductivity.

The actuator can deliver a large range of motion in a fraction of the time required by other devices due to the enhanced heat transfer produced by the particles. A Peltier cell was used for heating and cooling. This design can be used to fabricate microvalves and micropumps in contamination-sensitive LOC systems, as the membrane isolates the composite material from the environment. The presented design can be used in general to drive on-chip mechanical components in microelectromechanical systems, e.g. microswitches, grippers, variable capacitors, etc.

1.1 Overview of the problem

At present the operation of a typical microfluidic system depends on an external pneumatic circuit to control the fluid in the device, which considerably increases the size and cost of the system [16], [17]. Active electrically addressable microvalves offer the highest level of controllability, as they respond to external signals independently of the state of the fluid. Nevertheless, most internal actuation mechanisms, e.g. electrostatic, magnetic, thermopneumatic, piezoelectric, etc. cannot provide a large range of motion, for high open/close flow ratios; high closing pressure, for reduced leakage; and fast response simultaneously.

Phase change microactuators take advantage of the ability of some materials, e.g. sol-gel [18], hydrogel [19], paraffin [20], ice [21] and polyethylene glycol (PEG) [22], to undergo a significant volume change when they transit between the solid and liquid phases when temperature changes. Microvalves using the PC actuation mechanism have been implemented in numerous microfluidic devices, as they are easier to fabricate, stable and durable [23], [24]. They can also produce large forces and stroke distances. However, PC valves feature a very slow response, and this renders them unusable for applications where rapid valving is critical. Several PC microvalves have the additional disadvantage that the PC material gets in direct contact with the fluid, which produces cross-contamination [25].

1.2 Paraffin microactuators as promising actuators

Paraffin wax has remarkably high volume change ratios (10-30% [26]), and is available in melting temperatures between 41.6 °C and 150 °C [9], [7]; therefore, actuators of large range of motion can be built for various temperature environments. Paraffin is also chemically inert to many substances, including water, and does not decompose over repeated melting-solidification cycles [26], [27] which greatly extends the reliability and lifetime of the actuators. The main drawback of paraffin wax however, is its very low thermal conductivity (0.21–0.24 W/m-K [28]), so it offers a high resistance to accept or release heat. At the same time, paraffin has a very high specific heat capacity (2000 J/kg-K [27]) compared to other solids; thus it acts as a large energy container, wherein it is necessary to store large amounts of heat to reach the melting temperature, and similarly, it is necessary to release a large amount of heat for the material to solidify. In phase change actuators, the combination of these two factors produces slow mechanical response and waste of power, regardless of the size of the actuator.

1.3 Thesis Overview

This thesis deals with the design, fabrication, and characterization of a phase change microactuator that can be integrated into microfluidic systems for portable diagnostic systems. This microactuator takes advantage of the high volumetric

expansion of paraffin wax used as a phase change material sealed in a reservoir. Chapter 2 presents an overview of MEMS technology, and briefly reviews two main categories of microvalves. It also gives a survey on various kinds of microactuators.

Chapter 3 provides an overview of the basic design approaches, detailed fabrication steps, and characterization of the microactuator.

In Chapter 4, we demonstrate the synthesis method of the nanoparticles and also preparation of the nanocomposite used for actuation of the microactuator. At the end of this chapter, the characterization of prepared nanocompsoite is also discussed.

Chapter 5 discusses the thermal control system design, and also the testing of the overall system.

Chapter 6 provides the summary of the project, and also discusses possible future projects.

Chapter 2

Background overview

2.1 Design and Development of MEMS

Micromachining and micro-electromechanical system (MEMS) is the technology that can be used to produce complex microstructures by combining electrical and mechanical components [29]. MEMS utilizes fabrication technologies used in the integrated circuit (IC) industry to construct various mechanical components such as diaphragms and springs in order to make integrated and portable devices [30]. Some of the examples of MEMS technology include accelerometers, sensors, microactuators and fluid pumps [31]. Figure 2.1 shows some of these MEMS applications [32].

In the last 50 years, silicon has been used as the main substrate in the IC industry due to its many desirable electrical, mechanical and thermal properties [33], [34]. These excellent factors have also made silicon a very successful material in various microsensor and microactuators applications. The ability to fabricate micromechanical components from silicon has many benefits and one of the most important advantages is that when it is flexed there is virtually no hysteresis, hence there is almost no energy dissipation [35].

Even though silicon is the material of choice in industry, the high cost of crystalline silicon wafers and their complex production has led the industry to look at less expensive materials such as polymers that can be produced in huge volumes with a great variety of characteristics [36]. MEMS devices can be produced from polymers by various processes such as injection molding, embossing or stereolithography and are especially well suited to microfluidic applications such as disposable medical devices.
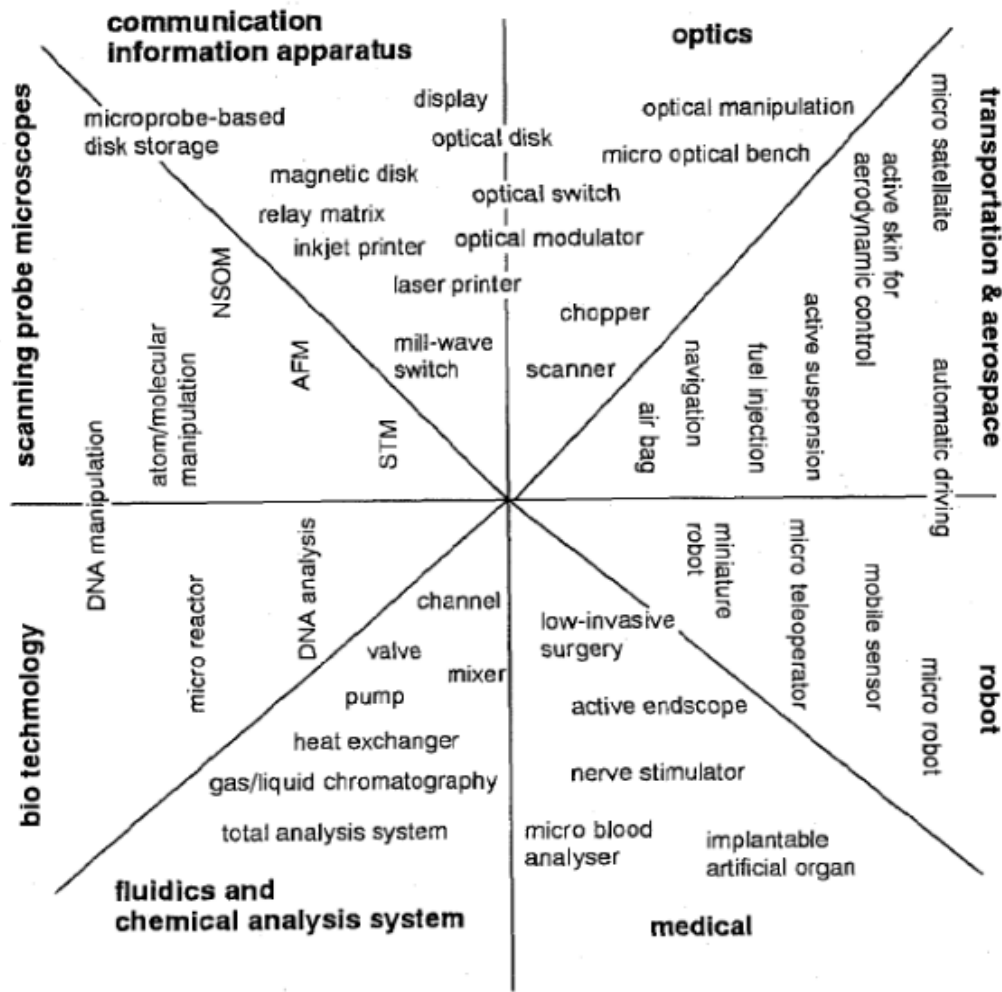
Figure 2.1: A map of MEMS applications [32].

2.2 Microfluidics

Microfluidics refers to devices with one or more channels with dimensions less than 1 mm that can manipulate a minute amount of fluids such as water, blood samples, protein and antibody solutions and bacteria cell suspensions [37], [38]. They are typically fabricated using a range of various substrates including silicon, glass and polymers such as poly methyl methacrylate (PMMA), polycarbonate (PC), poly ethylene terephthalateglycol (PETG), poly dimethyl siloxane (PDMS) and SU-8 using photolithography techniques [39].

Microfluidic devices have various kinds of applications including capillary electrophoresis [40], polymerise chain reaction (PCR) [41–43], DNA analysis [44–47], and protein and cell separation [48].

The use of microfluidic devices for biomedical research and clinically useful technology has significant advantages [49]. First, due to the small volume consumption of fluids within microchannels, usually several nanoliters, the amount of reagents and analytes used is very small. This is significant for expensive and precious samples and reagents in biological analysis. Second, the fabrication methods used to create microfluidic devices are relatively inexpensive and are capable of producing highly elaborate and multiplexed devices.

The implied promise of a microfluidic system is to integrate and miniaturize several different lab processes on the same substrate chip to create portable clinical diagnostic devices [50]. In 1990s, Manz et al. demonstrated one

of the first integrated systems to perform sample pretreatment, separation and detection on a silicon chip [51]. Since then there has been a growing interest on the integrated microfluidic-based diagnostics devices and promising approaches are in sight.

Integrated microfluidic systems would offer significant advantages of reduced sample and reagent volume consumption, low power requirements, faster reaction and shorter analysis time. All these advantages have led into point of care medical diagnosis, which is one of the most promising applications for microfluidic systems. Despite all these advantages and great advancements in the field of LOCs in the past few years, the major limiting factors are external optics, pumps or pneumatic control systems and external high-voltage power supplies [52]. These equipments are bulky and not portable and significantly increase the complexity and cost of the whole system.

2.3 Microvalves

Microvalves are one the most important control elements in the operation of microfluidic systems and are used to control routing, timing and separation of the fluid streams within these systems [53]. Although there has been a great progress in the performance of microvalves in the last 20 years, lack of reliable microvalves has delayed the successful miniaturization and commercialization of integrated microfluidic systems. Microvalves developed to date can be categorized as shown in table 2.1, and most of them are generally classified in the

form of active and passive microvalves using mechanical and non-mechanical moving parts [7].

Passive (check) microvalves are based on the surface tension effect. They only open to forward pressure and block fluid flow in reverse direction. Although these kinds of microvalves are easy to fabricate, they are not as diverse in their functionality as active microvalves. The main application of the passive microvalves or check valves is in inlets and outlets of the micropumps as mechanical moving parts [54].

However, active microvalves can open and close fluid flow based on an external signal regardless of the status of the fluid system. Most active microvalves consist of a flexible membrane actuated via electrostatic, electromagnetic, thermopneumatic, piezoelectric and shape memory means. Although active actuation microvalves offer the highest level of controllability and have good performance, most actuation mechanisms, e.g. electrostatic or magnetic, can not simultaneously provide a large range of motion for high open/close flow ratios, and high closing pressure, for reduced leakage and fast response. Moreover, they are usually more complex and more difficult to fabricate. As a result they are too expensive and also require high power consumption to operate. Consequently, they are not suited to practical point of care medical diagnostic applications [55].

Categories			
Active	Mechanical	Magnetic	External magnetic fields Integrated magnetic inductors
		Electric	Electrostatic Electrokinetic
		Piezoelectric	
		Thermal	Bimetallic Thermopneumatic Shape memory alloy
		Bistable	
	Non-mechanical	Electrochemical	
		Phase change	Hydrogel Solo–gel Paraffin
		Rheological	Electro-rheological Ferrofluids
	External	Modular	Built-in Rotary
		Pneumatic	Membrane In-line
Passive	Mechanical	Check valve	Flap Membrane Ball In-line mobile structure
	Non-mechanical		Diffuser
		Capillary	Abrupt Liquid triggered Burst Hydrophobic valve

Table 2.1: Classification of microvalves [7].

2.3.1 Active Microvalves

Active microvalves are common components in microfluidic systems and use actuators to regulate fluid in microchips. These microvalves fall into three major categories based on their actuation originality [7]. In the first category, mechanically active microvalves consist of a mechanically movable membrane coupled to magnetic, electrostatic, piezoelectric or thermal actuation mechanisms. The membrane deflects when the actuating sources is turned on; it seals against the valve seat and closes the valve or changes the channel geometry in order to control the fluid flow inside the channels. The various kinds of actuating methods have been depicted in Figure 2.2. The second category is non-mechanical active microvalves that use smart materials such as phase change or rheological materials and the actuation mechanism is based on the phase change, electrochemical, and rheological methods. Phase change actuation includes sol-gel, hydrogel and paraffin. Moreover, ferrofluids and electro-rheological material can also be employed in these kinds of microvalves. These valves have simple structures and may consist of a membrane, which moves due to the valving material. The third category is external active microvalves and includes pneumatically actuated valves and modular build in valves. These microvalves can produce high force and deflection; therefore, there won't be any leakage flow. However, in this actuation mechanism miniaturization is difficult due to the external systems [7], [55].
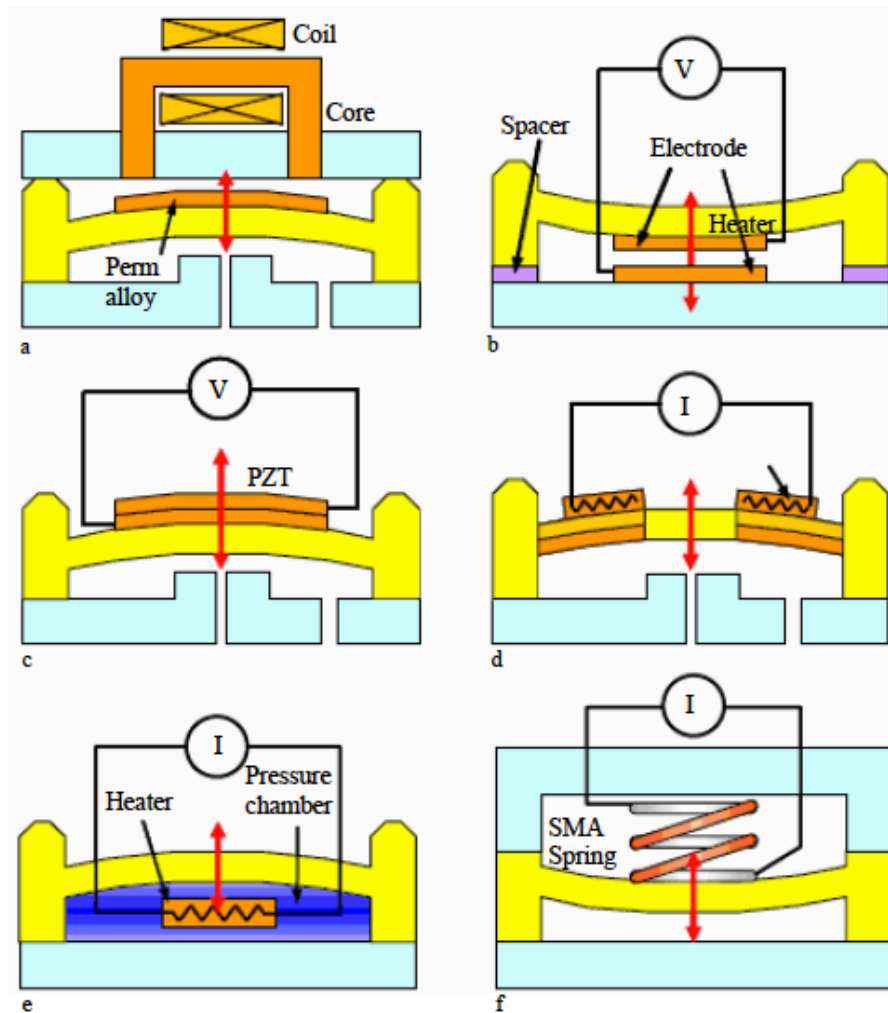
Figure 2.2: Illustration of mechanical active microvalves with (a) electromagnetic (b) electrostatic (c) piezoelectric (d) bimetallic (e) thermopneumatic (f) shape memory alloy actuation mechanisms [7].

2.3.2 Passive Microvalves

While active microvalves have complex structures and difficult to be integrated into portable systems, passive microvalves have been a subject of interest due to

their structural simplicity [56]. These kinds of microvalves are ideally suited for simple tasks, and allow fluid flow in only one direction. Passive microvalves normally consist of either a cantilever or a membrane on the silicon surface and are mostly categorized in one of three groups: 1) Silicon/polysilicon or polymer-based check valves 2) Passive valves based on surface tension effects, or 3) Hydrogel-based biomimic valves. Figure 2.3 depicts various kinds of passive microvalves [57].
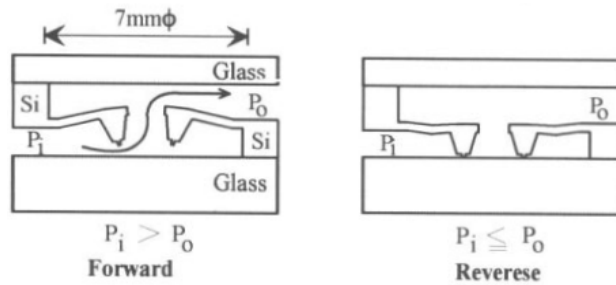
a) Membrane type with Mesa structure
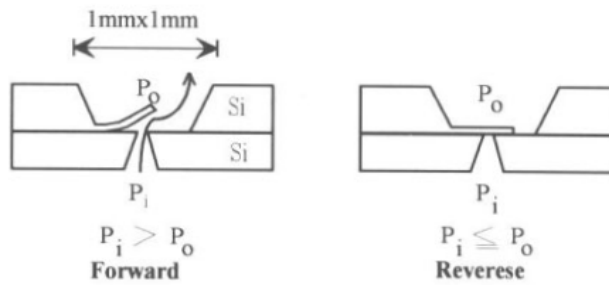
b) Cantliver or flap valve
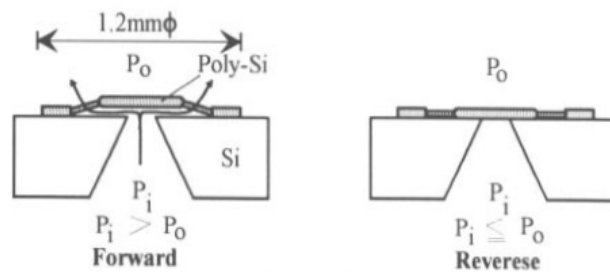
c) Polysilicon membrane

14
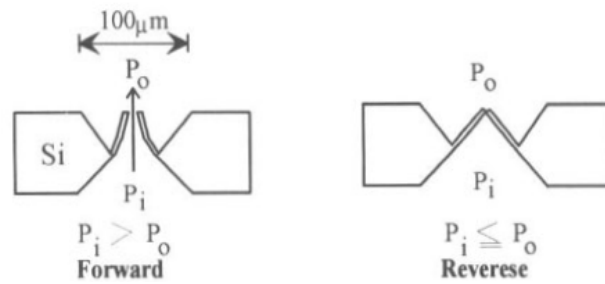
d) V-groove type
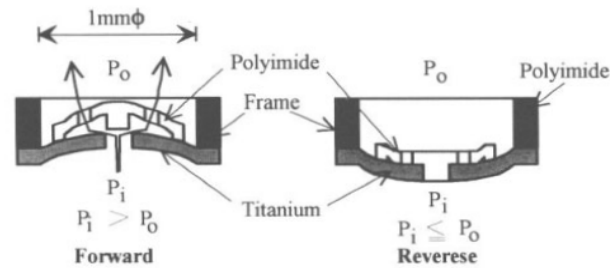
e) Titanium/polyimide membrane
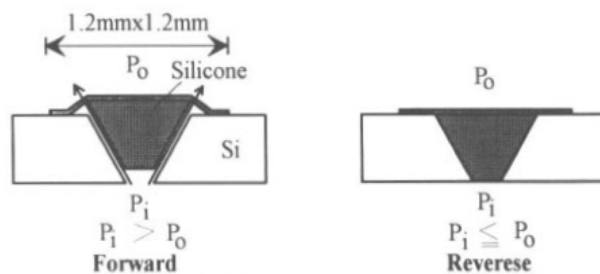
f) Silicone float valve

Figure 2.3: Schematic drawings of the passive microvalves [6].

2.4 MEMS microactuators

Actuators are used to transform nonmechanical input energy into mechanical output energy. Advances in miniaturization of mechanical, fluidic, thermal, optical, magnetic and chemical systems and devices have had dramatic impacts on

commercial profit and technological advances [8]. Development of actuation forms that can be implemented with the materials and technologies of silicon IC microelectronics is one of the important steps in the progress of microactuator technology. In this way microactuators would be compatible with microelectronics and microsensors fabrication technology, so they can be integrated with them to form a single on-chip or a hybrid-assembled system for future medical and biological applications.

Depending on the actuation principle, MEMS microactuators can be classified into two main groups: external forces and internal forces. In the first group the forces between the stationary and moving parts is produced due to thermopneumatic, electrochemical, electrostatic or magnetic fields; however, in the second group of microactuators, special materials with actuation capacities such as shape memory alloy, phase change and piezoelectric materials have been used to generate force [8]. There exists a wide range of materials that can be used for actuation. Maximum power consumption, response time, maximum force as a function of displacement, and dimensions of the actuator are important factors in choosing the right actuation mechanism. Below, four types of most important microactuators have been discussed.

2.4.1 Electrostatic Microactuators

Electrostatic actuation is a simple principle that uses electrostatic forces, which are the attractive forces that can arise between two parallel plates or elements with

opposite charges. These actuators are advantageous due to their simple structures, fast response times, and low power consumption. Moreover, another advantage of electrostatic actuators is that their fabrication method is compatible with standard IC micromachining processes [58]. This makes it possible to design VLSI fluidic systems with this actuators integrated [59]. Figure 2.4 shows two parallel plates with equal and opposite charges. Vectors in this picture show the electric forces, which tend to pull the upper plate and lower plate together. There are a variety of electrostatic microactuators fabricated with arrangements such as parallel plate capacitors and interdigitated finger or comb structures. Figure 2.5 shows a comb drive actuator that utilizes electrostatic forces that act between electrically conductive combs. It consists of interdigitated combs used to generate forces and motions.

By applying external voltage (V) to parallel plates, the electrostatic force (F) can be obtained from equation (1)

$$F = \frac{1}{2}C\frac{V^2}{d} \qquad (1)$$

Where;

$$C = \varepsilon_o \varepsilon_r \frac{A}{d} \qquad (2)$$

C is the capacitance between the plates, d is the distance of gap between the plates, ε_0 is the permittivity of free space, ε_r is the dielectric permittivity of the plates, and A is the surface area [58].
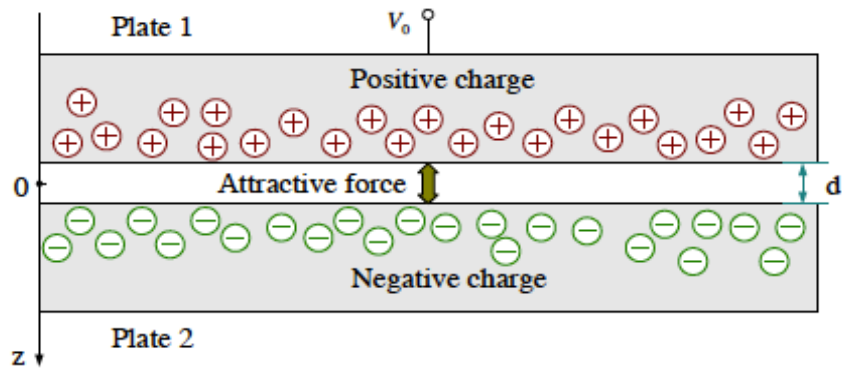
Figure 2.4: A physical model used to analyze electrostatic force [58].
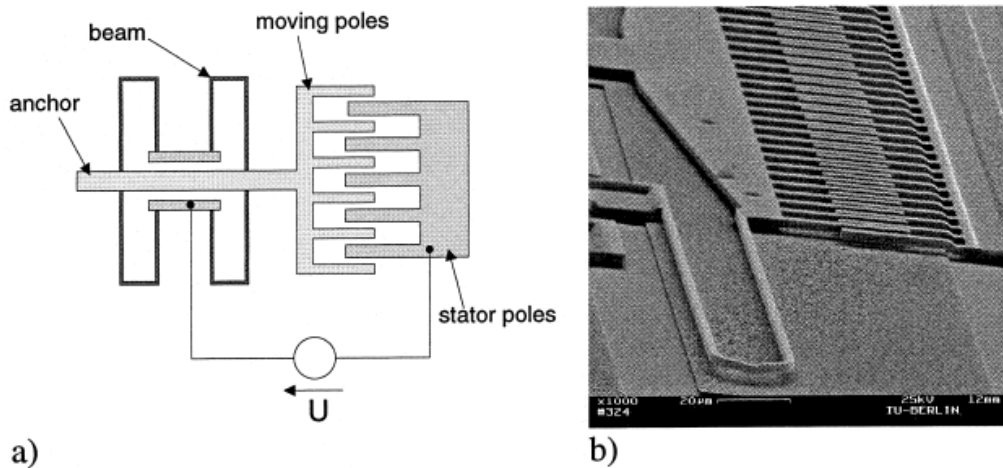
Figure 2.5: (a) Comb drive linear actuator (b) SEM picture of the comb drive [8].

2.4.2 Piezoelectric Microactuators

One of the commonly used methods for microactuators is piezoelectric actuation [60]. Piezoelectricity is the ability of certain crystals to stress or stretch in response to an applied electric field [61]. By applying voltage to piezoelectric materials, they can generate a large force even for small scales. However, due to

their high young's modulus, they provide only small deflection. Consequently, since materials with higher piezoelectric strain coefficient have a lower young's modulus, there is a trade-off between force and displacement when choosing a piezoelectric material [62]. There are various ways to overcome the drawback of the small strike of piezoelectric materials such as stacked piezoelectric discs, hydraulic amplification of the piezo and bimorph [7]. Piezoelectric force can be used for actuation in many applications, such as electric fans, hydrophones, microphones, inkjet printers, control valves, micropumps, tactile sensors, acoustic control and micromotors. Figure 2.6 shows a typical piezoelectric microactuator.

Rogge at al developed a normally closed polymer microvalve with a stroke of 50 μm using hydraulic amplification. In this design hydraulic transmission translated the disk displacement to move a valve membrane. Figure 2.6 shows a schematic of the microvalve. The response time was 2 ms, and it needs high voltages to drive the microvalve [63].
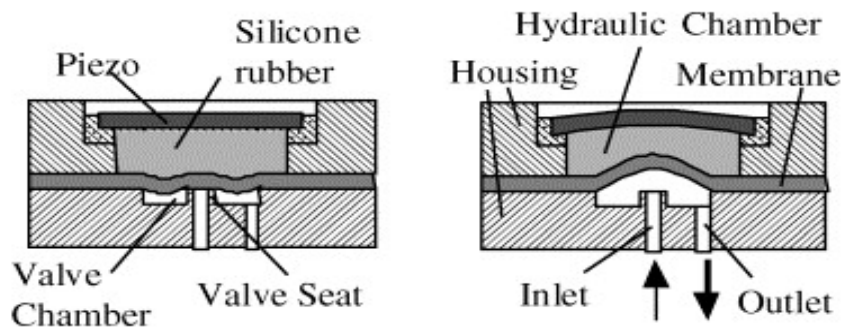
Figure 2.6: Schematic of the microvalve with piezo in closed state (left) and open state (right) [63].

19

In another work, Watanabe and Kuwano [61] demonstrated a piezoelectrically actuated valve. In this design a film of piezoelectric material was deposited on a movable membrane. Application of electric potential to the piezoelectric film transmitted to the membrane and deformed it.

2.4.3 Phase-change Microactuators

By using the pressure resulting from the solid to liquid phase transition of the active materials such as paraffin, hydrogels an ice in mechanical actuators both a large force and a large expansion can be created. This force resulted from volumetric expansion of the material can be utilized to create linear motion and large stroke deflection of a membrane.

The force, stroke length and response time of PC paraffin microactuators are highly dependent on the relative size of the actuator and its heating/cooling system. The response time is also defined in different ways and it is different for the heating and cooling ramps. Because of this it is difficult to establish a standard of comparison.

Klintberg et al. [64], for instance, reported a large PC diaphragm actuator of 68 mm diameter and 825 μm thickness, fabricated in Si and filled with paraffin. The device, heated externally by contact with a copper cylinder, was capable of moving a 3 N load with 75 μm displacement; the response time was 15 s for full range actuation and the maximum displacement without a load was 90 μm at

80 °C. Because of its size, this design is not suitable for microvalve applications in LOC systems, but is an excellent example of how strong a PC actuator can be.

To reduce response time, Carlen et al. [65] produced small 200-400 μm radius diaphragm actuators in Parylene, filled with a 9 μm layer of paraffin; and dramatically increased the power input by using a thin film integrated heater in direct contact with the paraffin. The devices attained response times of 30 to 50 ms and power consumption levels of 100 to 150 mW. The tradeoff for this tremendous reduction of size was a diaphragm displacement of only 2.7 μm. This small stroke is due to the small volume of paraffin used and the small dimensions of the diaphragm, as the maximum displacement of a clamped diaphragm subjected to uniform pressure decreases with the fourth power of its radius.

Although the size of these microactuators is appropriate for a microfluidic device, their fabrication process is complicated, as Parylene is not a photo-patternable polymer; and their stroke distance is insufficient, since microchannels in LOC systems are typically in the order of 10–100 μm height or more to handle the minimum necessary volumes of sample and reactants.

A different approach to decrease the response time consisted in mixing graphite particles with paraffin [66], which created an electrically conductive material, and this made it possible to heat the paraffin directly with an electrical current. The actuator using this material consisted of a 6 × 6 mm^2 diaphragm of 45 μm thickness, and achieved a response time of 5 s, with full deflection amplitude of 17 μm. Adding graphite to paraffin could have also increased its

thermal conductivity, however for this to produce a useful effect, mixing would need to by highly uniform. In addition, graphite's thermal conductivity is anisotropic [67], and hence the effect of lower thermal conductivity could probably be observed only in certain geometrical arrangements of the system.

Park et al. [68] recently reported a phase change microvalve based on iron oxide nanoparticles dispersed in paraffin wax. The particles were used as nanoheaters that sourced heat when irradiated with a laser, owing to the high light absorption of iron oxide. When the paraffin melts, it bursts into the microchannels and blocks flow. In this example, the working fluid comes in direct contact with the mixture, so it can easily be contaminated with iron oxide, which is unacceptable for genetic analysis and medical diagnosis applications. This approach also requires external optical instrumentation and excitation components that are not compatible with miniaturization. Furthermore, iron oxides are characterized by their low thermal conductivity (7.0 W/m-K @ 304 K for Fe_3O_4 [67]). Therefore the addition of these nanoparticles does not improve the thermal properties of paraffin.

2.4.4 Pneumatic Microactuators

Pneumatic microactuators are applied in all kinds of microfluidic systems in order to control, mix and pump fluids. These microactuators play an important role in medical applications where high actuation force and large strokes are required [69].

Takao et al presented a pneumatically actuated silicon microvalve, which worked as a transistor-like device for a functional microfluidic circuit. In this design, a silicon membrane functioned as the gate of the transistor controlled by external pneumatic air pressures, while the inlet and outlet served as the source and the drain.

In another work, Mathies' group developed a practical pneumatic microvalve with latex membranes to create a fully integrated PCR-CE microfluidic device as shown in Figure 2.7. In this system, two aluminum manifolds, one for the vents and one for the valves, were placed onto the ports and clamped by applying vacuum. These manifolds were then connected to external solenoid valves for pressure and vacuum actuation. Samples were loaded from the inlet by opening the valve using vacuum (4 kPa) and forcing the sample under the membrane using pressure (69-83 kPa). The samples stopped at the vent, and the valve was pressure-sealed in order to enclose the sample [7], [42].

Pneumatically-actuated PDMS membrane microvalves have also been reported by several groups. Ohori et al [70] developed a three way microvalve for whole blood handling. This valve was advantageous due to easy assembly, large on/off flow ratio, no bubble problem and low cost due to the partly disposable structure. Another three-way pneumatically driven but normally closed microvalve was presented by Hosokawa and Maeda [71]. This microvalve was composed of three independent one-way valve units. Each valve had a separate 25 μm thick PDMS membrane actuated by external negative pressure. In order to

open the valves and fluidic routes a negative pressure of 60 kPa was applied by an

external vacuum pump.

(a)

(b)
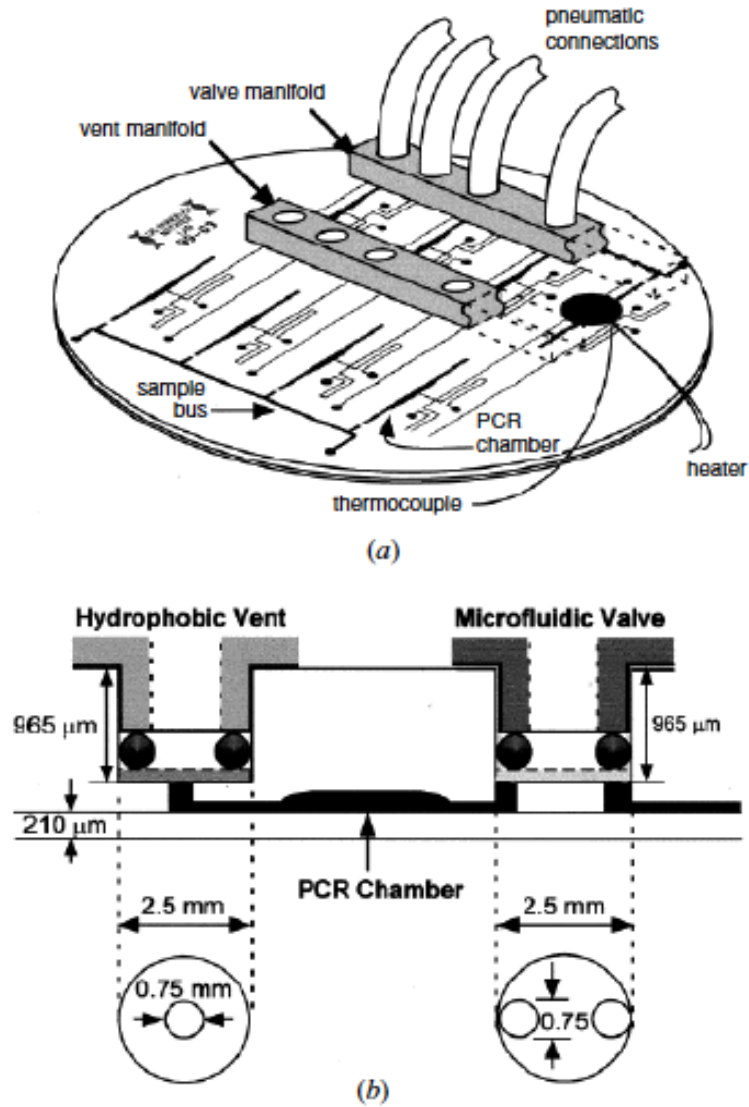
Figure 2.7: (a) Microfluidic PCR-CE device (b) Pneumatically actuated microvalves and hydrophobic vents [42].

Chapter 3

Microactuator Chip Design, Fabrication flow, and Measurements

3.1 Device Design

3.1.1 Device Structure

This actuator was fabricated from two layers of SU-8 (a photo-patternable epoxy-based resist), joined by thermo-compressive bonding on a glass substrate (Figure 3.1). The bottom layer contains the reservoir and channels that connect it to the inlet and outlet ports. The top layer forms the membrane that seals the reservoir cavity. At the end of the process, this layer is punched to open access to the channels in the bottom layer. SU-8 is a biocompatible polymer that can be easily photo-patterned to fabricate microchannels and other structures. Paraffin easily fills the reservoir through its access channels by capillary action, owing to the high wettability of SU-8 to paraffin. SU-8 was also chosen because of its low thermal conductivity (0.2 W/m-K), which reduces heat loss from the reservoir to the ambient. SU-8 also possesses a very low Young's modulus (4.95 ± 0.42 GPa [72]), compared to materials like silicon, which allows a large deflection of the membrane without deforming plastically or tearing.
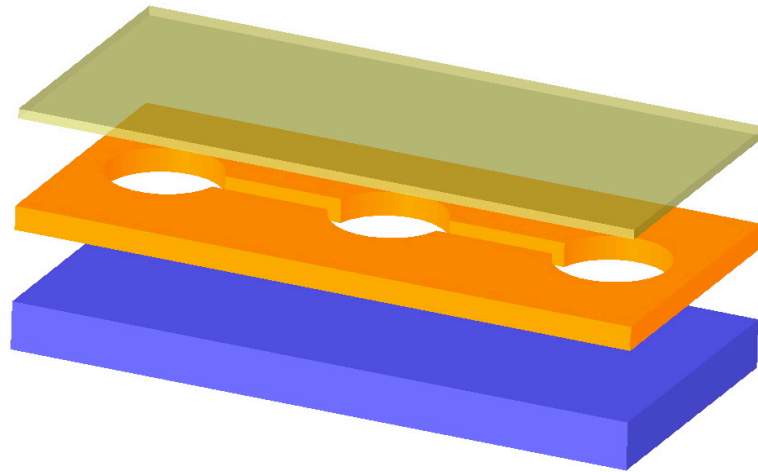
(a)
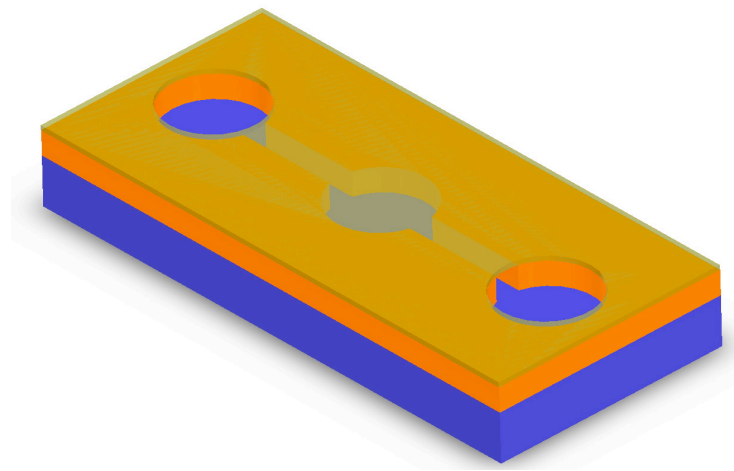
(b)

Figure 3.1: schematic drawing showing (a) two layers of SU-8 on a glass substrate (b) SU-8 layers are bonded together using thermocompressive bonding method.

Figure 3.2 is a cross section schematic of the microactuator, which shows the reservoir and the flexible membrane. Controlling the temperature under the melting point of paraffin, the mixture solidifies, contracts and pulls the membrane down. The membrane also deflects upwards due to volumetric expansion of the

melted nanocomposite in the reservoir, which occurs when the temperature is above the melting point.
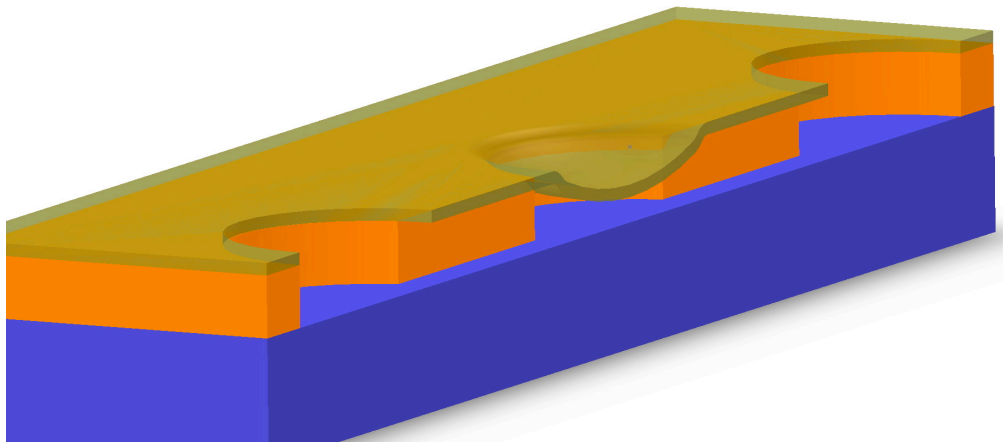
(a)
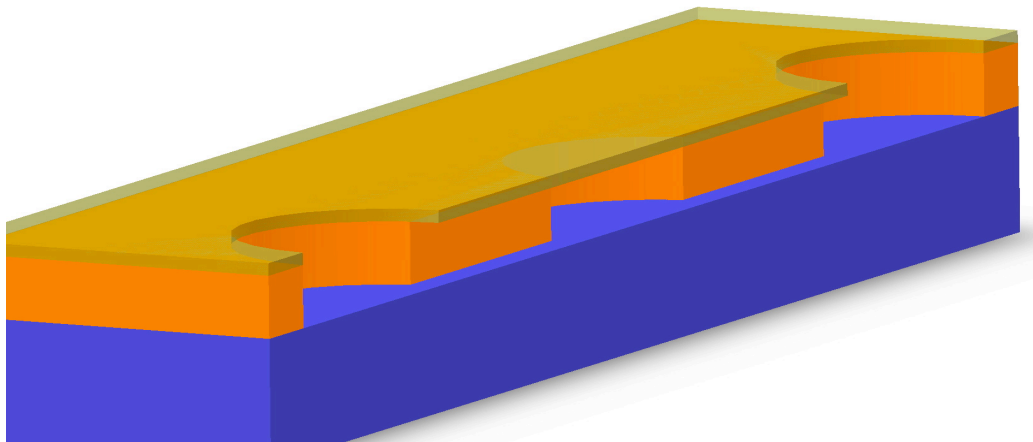
(b)

Figure 3.2: Schematic cross section of the microactuator. (a) recessed position – when the composite is solidified it creates a negative pressure; (b) advanced position – on melting the composite applies a positive pressure.

The molten paraffin does not flow out of the reservoir, because heat is locally applied in the reservoir region, thus the paraffin outside remains solid, and the channels are long enough to offer a very high resistance.

3.1.2 Material Selection

The selection of the materials is a key issue in MEMS. In BioMEMS, not only should the materials be compatible with each other during the fabrication process, but also biocompatibility of the materials and the surfaces are critical issues to consider.

SU-8

SU-8 is a negative, photopatternable, epoxy-based photoresist used as a structural material for MEMS and bio-applications. SU-8 has been used in fabrication of high aspect ratio structures up to 25 with standard contact lithography. It can also be possible to have film thickness from a few μm to a few hundred μm. Each SU-8 molecule contains 8 epoxy groups where each epoxy group can react with each other and form a polymer. SU-8 consists of three basic components: epoxy resin such as EPON SU-8, solvent called gamma-Butyrolactone (GBL), the photoacid generator from the family of the triarylium-sulfonium salts. This photoresist can be spin-coated on the substrate, and the film thickness is determined by the spin speed and the viscosity of the photoresist. Followed by

spinning on the substrate, photoresist is soft baked to evaporate the solvent. Upon UV exposure, SU-8 generates a strong acid ($HSbF_6$). Post exposure bake (PEB) step activates $HSbF_6$. The photogenerated acid catalyzes the reaction between the resin and the crosslinking agent, which causes the epoxy groups to selectively cross-link in the exposed areas and produce a highly cross-linked polymer. A development process in solvent-based developers can be used to dissolve the unexposed areas that are not cross-linked. Though SU-8 is used as a building material for MEMS, it is greatly dependent on the experimental conditions and equipment.

3.2 Fabrication overview

The microactuator is formed by stacking two layers of SU-8 on a glass substrate called the *device wafer*. The bottom layer is patterned with cavities and channels directly onto the device wafer, while the roof layer is patterned on a *carrier wafer* and then transferred onto the bottom layer by thermo-compressive lamination bonding. The carrier wafer is coated with PDMS, which adheres weakly to SU-8. The adhesion of SU-8 to PDMS is sufficient to hold the roof layer during processing, but low enough to allow releasing of the carrier wafer after bonding. The second layer is transferred onto the patterned SU-8 layer, forming sealed channels. The fabrication process is depicted in Figure 3.3. It comprises the following main steps:

1. Wafer preparation: a carrier and device wafer are cleaned and dehydrated. A PDMS film is formed on the carrier wafer.

2. SU-8 layer fabrication: the bottom layer is deposited and patterned on the device wafer. The roof layer is patterned on the carrier wafer.

3. Bonding: the layers are brought together and pressed while temperature is increased. After bonding the carrier wafer is released, leaving the finished structure on the device wafer.
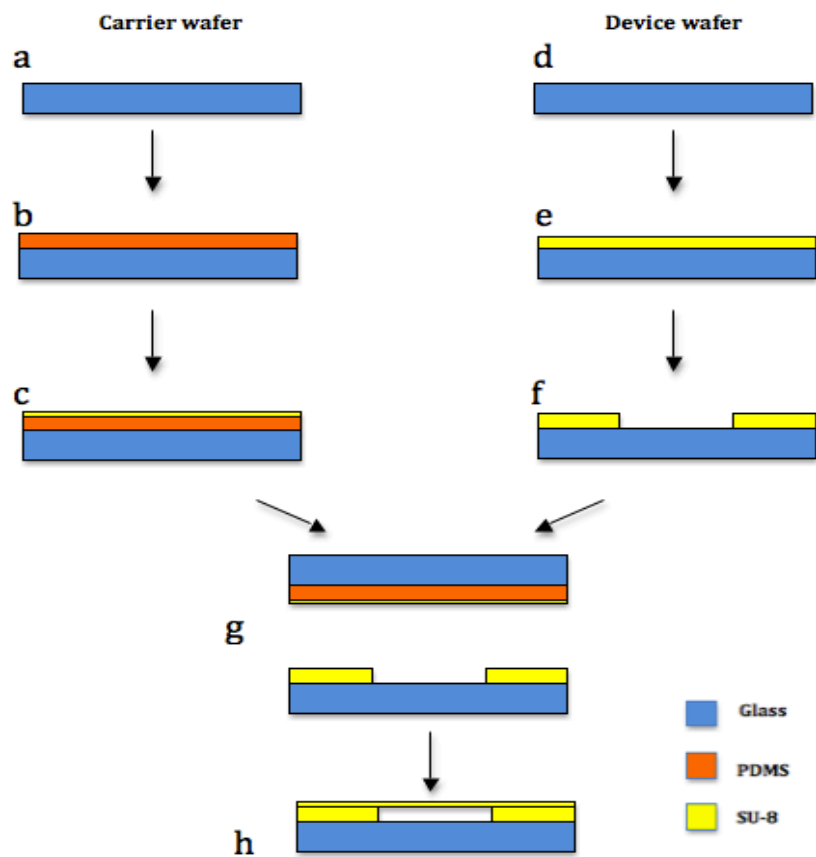
Figure 3.3: Microfabrication process flow shown in cross-section: Wafer preparation (a), (d); Spin coating of PDMS (b) and SU-8 (e); Photolithography (c), (f); Bonding of the photopatterned layers (g); and PDMS releasing (h).

3.3 Detailed Fabrication Process

Materials

- 1 x 100 x 100 mm (LxWxH) borofloat substrate (Paragon Optical Company, PA, USA)

- SU-8 2010 negative photoresist (MicroChem Corp., MA, USA)

- SU-8 Developer (MicroChem Corp., MA, USA)

- Sylgard 184 PDMS base/curing agent (Dow Corning, NC, USA)

- Chrome mask created using a pattern generator (DWL 200, Heidelberg Instruments, Heidelberg, Germany) in the University of Alberta Nanofab

SU-8 Process

1. Wafer Preparation

To increase the process reliability, the substrate should be cleaned and dried. The borofloat glass substrate should be cleaned in a fresh 3:1 (H_2SO_4:H_2O_2) Piranha solution for 30 minutes followed by rinsing in deionised water. After cleaning the substrates, drying with N_2 and dehydration by hotplate at 200 ˚C for 15 minutes is recommended. Then the substrate should be placed on the desk to cool down to room temperature for at least 30 minutes.

2. SU-8 Spin-coating

Take the appropriate chuck. Place the substrate in the spinner and in the center of the chuck. Apply SU-8 to the center of the substrate directly from the bottle. Set the spin speed for desired thickness. Dispense approximately 1 ml of SU-8 per inch of the substrate. After applying SU-8 spin to spread out the SU-8. To achieve a film thickness of approximately 10 μm, spin coat the SU-8 (with the lid on the spinner) as follows:

- 0 to 100 rpm@10 rpm/s

- 100 rpm, 5 seconds

- 100 to 500 rpm @ 100 rpm/s

- 500 rpm, 5 seconds

- 500 to 1500 rpm @ 300 rpm/s

- 1500 rpm, 30 seconds

- Coating should be done immediately after the wafer preparation step in order to avoid re-adsorption of any contamination.

- After spin coating SU-8 on the substrate, edge bead happens. Edge bead in SU-8 is a significant issue due to its high viscosity. Therefore, there would be an air gap between the top surface of the SU-8 and the mask, which may cause light scattering as it passes between the mask and the surface and decrease the image resolution. Therefore this gap should be minimized. Especially in the case of coating a thick photoresist, this could be even worse. Since the

nanofab does not have a bead removal system, a two step coating solution was used to lower the edge bead. In this method, the substrate is coated with the first layer of SU-8 and then, after the soft baking of the first layer, the second layer is applied on top of the first layer. In this way edge bead would be reduced and the surface is made flat enough for bonding.

3. Soft Bake

The SU-8 film is soft baked to remove solvent. A two-step soft bake by hotplate at 65°C and 95°C is used. In the developed protocol the substrate with 10 μm thick SU-8 is baked for 3 minutes at 65°C and 5 minutes at 95°C. Cool down the substrate to room temperature for 15 minutes.

- Using convection oven for this step is not recommended because a skin may form on the surface of the resist, which can inhibit the solvent's evaporation.

- After this step it is better to leave the photoresist to rest and stabilize for 1 hour or more.

4. Exposure

Expose the substrate to UV light using a mask aligner system (AB-M Inc., Silicon Valley, CA, USA). For a 40 μm film, MicroChem recommends an exposure dose of (150 to 160)*1.5 (glass) = 225 to 323 mJ/cm^2. Exposure time is calculated by dividing the exposure dose by the average power density of the UV lamp at 365 nm.

- In order to reduce the reflection, the borofloat glass substrates used are coated with a tin (Sn) film.

5. Post Exposure Bake (PEB)

Crosslinking of the exposed region of the SU-8 happens during the PEB. PEB should be done immediately after UV exposure in order to prevent the photogenerated acid to diffuse into the adjacent unexposed regions leading to the crosslinking reaction. Bake the substrate for 2 minutes at 65°C and 5 minutes at 95°C for a 40 μm thick photoresist. Leave the substrate to cool down to room temperature for 30 minutes.

6. Develop SU-8 Photoresist

In order to remove the unexposed SU-8, a development step is necessary. MicroChem's SU-8 developer is used to develop SU-8 film. Pour some SU-8 developer into a Pyrex dish. Place the substrates in the developer and move continuously. Rinse the substrate with IPA and dry with N_2.

PDMS as a sacrificial layer

1. PDMS Mixing and Degassing

The Sylgard 184 PDMS is a two-part mixture including base and curing agent. The two compounds are mixed with a volume ratio of 10:1 (v/v) with a plastic

dropper. For approximately 50 μm thick PDMS, 10 g of PDMS base and 1 g of PDMS curing agent is required. PDMS is mixed and then degassed in the vacuum oven at -25 in·Hg for 30 minutes to remove trapped air bubbles that were created during mixing.

2. PDMS Casting and Curing

Take the appropriate chuck. Place the substrate in the spinner and in the center of the chuck. Apply mixed and degassed PDMS to the center of the substrate directly from the bottle. Set the spin speed for desired thickness. Dispense approximately 1ml of PDMS per inch of the substrate. After applying PDMS spin to spread out the PDMS. To achieve a film thickness of approximately 50 µm, spin coat the PDMS as follows:

- 0 to 500 rpm@50rpm/s

- 500 rpm, 300 seconds

- After spinning, PDMS should be cured in the vacuum oven. Place the PDMS in the oven for 2 hours at 80˚C. After the curing is complete, remove the substrate from the oven and let it cool down to room temperature.

Device fabrication

The bottom layer on the device wafer is made up of two sub-layers, one of 15 μm and one of 25 μm thickness in this order to obtain a 40 μm thick film. This

subdivision has the purpose of reducing the height of the beads left at the edge of the wafer during the spinning process. The growth of the edge beads exacerbates when spinning high viscosity polymers like SU-8, and beads may grow even taller when spinning very thick layers.

The first layer is fabricated by spinning approximately 1 ml of SU-8 2010 per inch of the substrate, at increasing speed, in several steps from 100 rpm (5 s) up to 1500 rpm (30 s). This process is performed right after wafer cleaning and drying in order to avoid re-adsorption of water and particle contamination. After spinning, the wafer is soft-baked on a hot plate at 65 °C for 3 min and then at 95 °C for 5 min. The wafer is allowed to reach room temperature, and then the second sub-layer is spun with the same parameters as for the first one, but reaches higher thickness. The wafer is baked again at 65 °C for 5 min and at 95 °C for 8 min to remove solvent from the second layer. After soft-bake of the second layer the wafer is exposed to 365 nm UV light for 1s through a Cr mask, in a contact lithography system, with a 293 mJ/cm^2 dose.

Both sub-layers are cross-linked together with a post-exposure bake (PEB) at 65 °C and 95 °C for 2 min and 5 min, respectively. The film is then developed in SU-8 developer for 2 min with agitation; and then rinsed with IPA and dried with N$_2$.

The roof layer is fabricated on the carrier wafer by spin-coating SU-8 on PDMS. This process is critical since the adhesion to PDMS must be low enough to allow release, but at the same time high enough to hold the SU-8 layer along

the process and avoid the dewetting effect. This effect results in surface non-uniformities or complete collapse of SU-8 under its own surface tension. This effect can be controlled by soft-baking on a temperature ramp. Instead we sputtered a ~10 nm gold layer on the PDMS, which renders the surface hydrophilic to SU-8 and prevents any degree of dewetting, while allowing wafer release.

After this treatment a $10\,\mu$m thick roof layer is spun and soft-baked at 65 °C for 10 min and 95 °C for 10 min on a hot plate, and then exposed to UV light. Thereafter, the film is partially cross-linked by post-baking at 60 °C for 5 min and 85 °C for 5 min. The temperature in the second step is set 10 °C less than the typical SU-8 cross-linking temperature in order to leave free surface monomers that will crosslink together with the polymer chains at the surface of the bottom layer during bonding.

Bonding

The roof layer is joined to the bottom layer and then pressed with a force of 20 kN in a hot-embosser in vacuum. The temperature in the embosser is elevated to 100 °C for 900 s to cross-link together the SU-8 layers. The degree of cross-linking of the roof layer is optimized so that the structures withstand pressure without deforming and at the same time ensure good bonding yield and strength. After bonding, the carrier wafer is removed, leaving gold on the surface of the structure.

3.4 Results and Discussion

3.4.1 Fabrication Process

- **SU-8 Protocol Development**

SU-8 is a multifunctional and well recognized polymeric photoresist, however, there are several processing parameters that need to be carefully tuned, such as exposure dose and temperatures of prebake and post bake. Figure 3.4 shows some of the experimental results for various exposure doses.
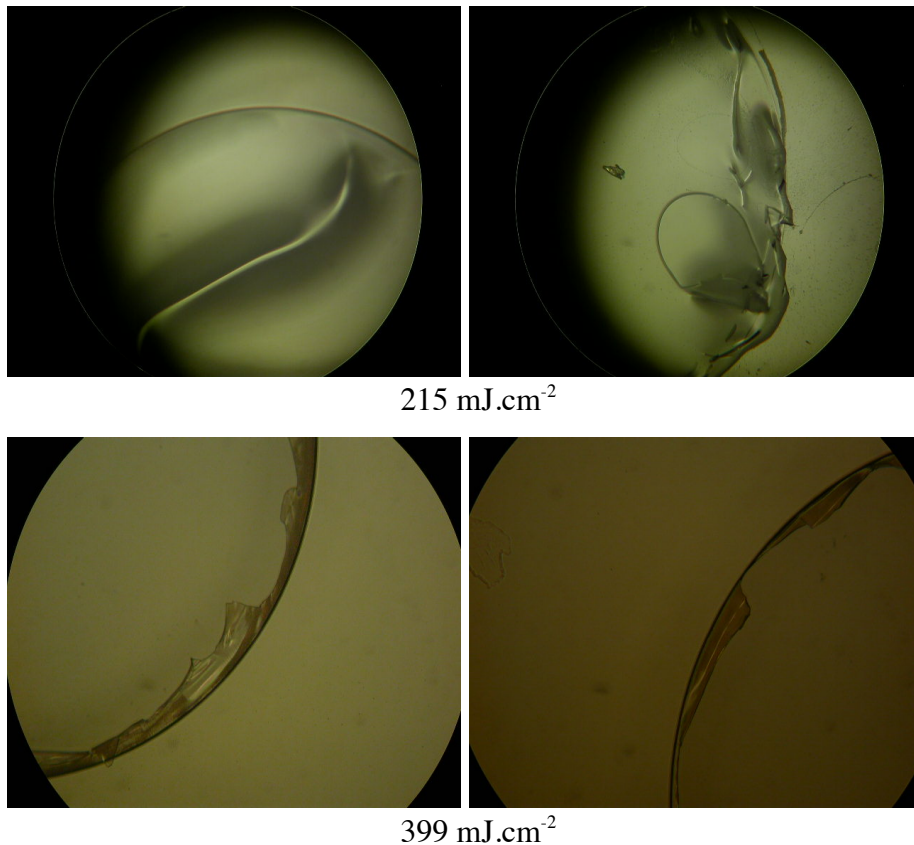

215 mJ.cm^{-2}

399 mJ.cm^{-2}

Figure 3.4: Examples of failed fabrication results for various exposure doses.

Despite testing a wide range of exposure doses, as it is shown in Figure 3.4, we couldn't pattern channels and wells with sharp edges. After investigating various parameters, we came to the conclusion that SU-8 is highly sensitive to blue visible light, and it has a negative impact on the results. As SU-8 spin-coater and hotplates are located within an area of the cleanroom that has no UV filtering, samples were exposed to the light forming partially cross-linked SU-8 on the hot plate and during spin-coating and soft-baking process. After covering the samples in every step of the process, we succeeded to get following results (Figure 3.5).

Figure 3.5: Experimental results with optimized protocol.

• **PDMS Dewetting Effect**

PDMS was used as a sacrificial substrate material for releasing SU-8 structures. One of the challenges in the fabrication process was dewetting effect of SU-8 on the hydrophobic PDMS, which caused difficulty in spin coating SU-8 onto the surface. The reason for this effect is due to the low surface energy of the PDMS (~ 23 mN m^{-1}) and nonpolar methyl groups on surface of the PDMS. It has been reported in the literature [73] that brief O_2 plasma treatment of the PDMS surface

could temporarily alter the surface by increasing the concentration of the hydroxyl group and render it hydrophilic. This treatment is not permanent and can decay within a few hours. Figure 3.6 shows the effect of the O_2 plasma treatment on the surface of the PDMS.

(a)   (b)
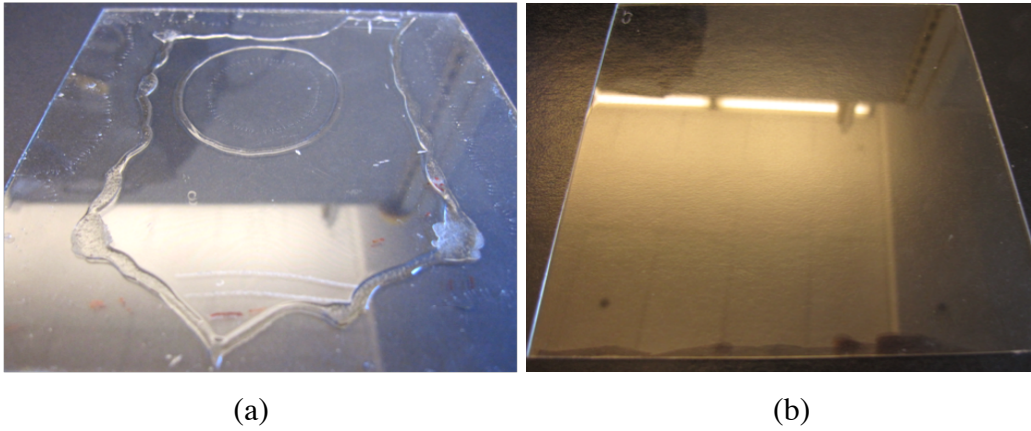
Figure 3.6: PDMS substrates a) before plasma treatment (b) after plasma treatment.

Although plasma treatment changes the PDMS surface and allows uniform coating of the SU-8, it could not be used in our fabrication process since SU-8 got stuck to the surface and could not be released after bonding (Figure 3.7).
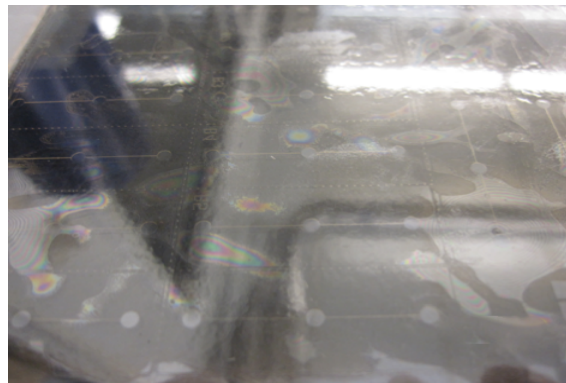

Figure 3.7: Bonding result after plasma treatment of the PDMS surface.

- **Surface Flatness**

Surface flatness is another important issue when fabricating macro and micro components, and a good surface smoothness is essential for fabricating a microactuator. It is one of the most important factors affecting successful bonding. It is also critical in obtaining uniform exposed patterns during the exposure step. Surface flatness errors hinder conformal contact between mask and the resist surface in contact lithography causing light diffraction and severe profile distortions. The surface nonuniformity gets worse as the thickness of the resist increases. Using a less viscous and multilayer photoresist greatly contributed to improve the surface flatness.

- **Bonding**

There are various bonding methods reported in the literature for fabrication of polymeric substrates, such as microwave bonding, bonding using adhesives, plasma activation, lamination and direct bonding. Two bonding methods have been tested in this project: thermal direct bonding and thermocompressive lamination bonding using hot embosser. In thermal direct bonding, two partially cross-linked SU-8 substrates are manually bonded together on the hotplate followed by exposure and post exposure bake. Although this method is simpler compared to other methods, the yield was very low. Thermo compressive bonding is the most commonly used method. In this method substrates are heated

to a temperature near cross-linking while applying pressure via hot embosser to increase the contact forces. The combination of pressure and temperature cause interfusion of the polymers' chains between surfaces. By controlling the temperature, a strong bonding between the mating contacts of the SU-8 substrates can be made, and bonding strength increases by molecular entanglements of the polymers. As shown in Figure 3.8, the first method has proven to be unsuccessful and the yield was about 30%. On the other hand, thermocompressive bonding by precisely controlling bonding temperature and force was completely successful and a high bonding yield (~100%) was achieved.

(a)   (b)
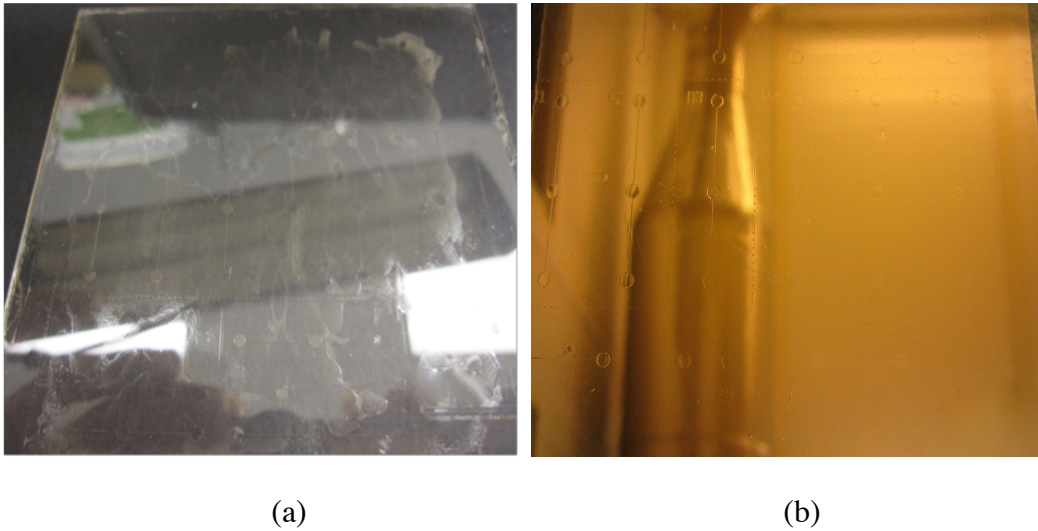
Figure 3.8: Bonding results (a) thermal direct bonding (b) thermocompressive lamination bonding.

3.4.2 SEM Results of the Fabricated Microactuator

We obtained 10 μm thick free-standing and very flat membranes, as depicted in Figure 3.9, over 2 mm diameter and 40 μm depth reservoirs, which can allocate

125.7 nL of melted nanocomposite. The bonded area was nearly 100 %. The

bonding strength passed the tape test and survived dicing without delamination.
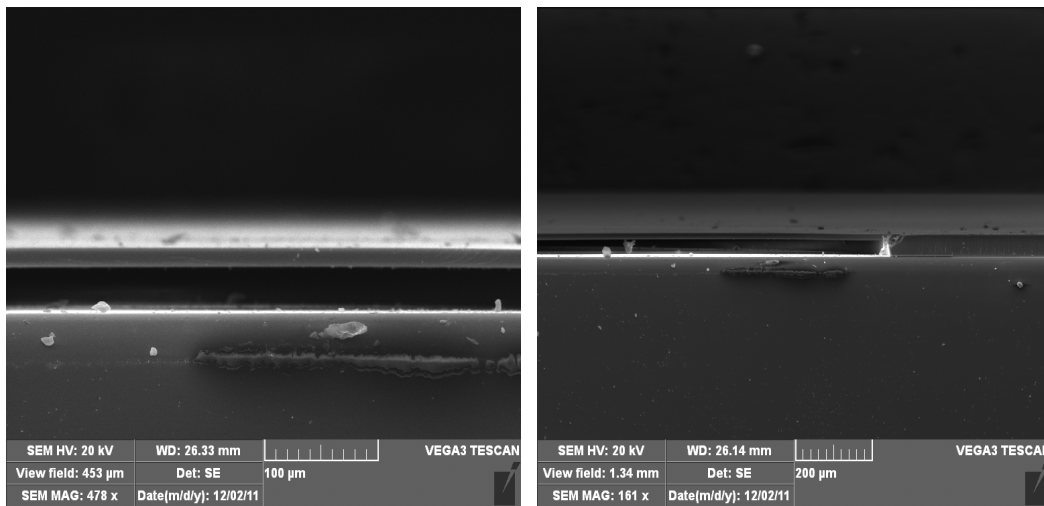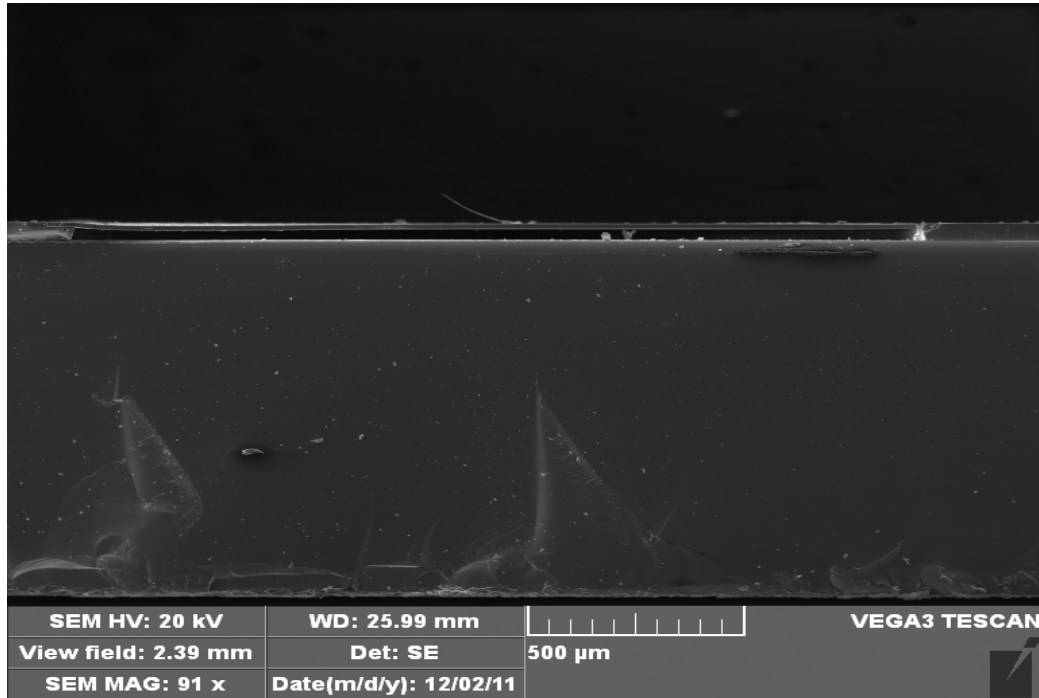
Figure 3.9: SEM cross-section micrographs of the fabricated microactuator before

filling in the nanocomposite.

Chapter 4

Microcavity Nanomaterial Development

4.1 Cavity Design and Materials

The polymer microactuator employs the phase transition of a nanoparticle-paraffin composite to produce mechanical force and motion. The actuator consists of a reservoir containing the phase change compound enclosed by a flexible membrane isolating this material from the working fluid, in order to prevent contamination. Specifically, gold nanoparticles were embedded in paraffin to accelerate the heat transfer and melting/solidification process. Gold has a very high thermal conductivity (317 W/m-K @ 300 K [67]) compared to paraffin (0.21–0.24 W/m-K [28]), thus gold nanoparticles in an adequate concentration may dramatically increase the net thermal conductivity of paraffin without hindering its ability to expand and contract. In this way, the compound may accept or release heat much faster than pure paraffin. This enhancement of the thermal conductivity of paraffin, combined with the extremely small volume of the reservoir (1 mm radius, 40 μm height, 125.7 nL volume), can potentially result in a quick deflection of the membrane.

4.2 Synthesis and Characterization of Nanoparticles

4.2.1 Preparation of Gold Nanoparticles

Three types of gold nanoparticles were prepared as follow [74]:

One hundred microliters solution of 0.05 M $HAuCl_4.3H_2O$ in 1.0 M aqueous HCl was added to 10 mL of deionized water. The solution was mixed with vigorous stirring, and the color would turn into bright yellowish. Then 100 μl solution of 0.05 M $NaBH_4$ in 1.0 M aqueous NaOH was added slowly, during this step the solution color turns intensively-red. After stirring, 5 g of acetone was added and mixed manually for several seconds. The solution of 0.1 g dodecanethiol in 5 g of toluene was added rapidly and mixed manually for 30 s (Sample F). The solution of 0.0147 g paraffin wax (Sigma-Aldrich, product no. 327204, St. Louis, MO) in 5.8 ml toluene was added rapidly and the mixture was shaken manually for 30 (Sample G). The solution 0.0155 g of solution paraffin in 5.8 of toluene and 0.118 ml of dodecanethiol was added rapidly and the mixture was shaken manually for 30 (Sample H). The mixtures were then left on the desk to allow the water and toluene layers to separate well one from another. After that, the layer of toluene was removed. The procedure was repeated for several times, and all the collected toluene layers were combined together. AuNPs were stored at 4-5 ˚C.

45

4.3 Synthesis and Characterization of Nanocomposite

4.3.1 Preparation of Nanocomposite

Paraffin wax is a mixture of saturated alkanes and hydrocarbons and it doesn't mix with polar fluids. It changes its volume at phase transition and the heat needed to change the phase is stored as latent heat and is returned when it crystallizes. Gold nanoparticles and other metals significantly change its thermal properties. In order to investigate the influences of the Au nanoparticles on the thermal conductivity of the paraffin wax differential scanning calorimetry (DSC) was used. In addition, Transmission electron microscopy (TEM) and ultraviolet-visible spectroscopy have been used for further investigation of the nanoparticles and show how nanoparticles embedded in paraffin wax can affect the thermal conductivity.

The integration of gold nanoparticles into paraffin to form a true nano-composite was a major challenge in this research, because paraffin is highly inert and hydrophobic, thus it does not allow simple dissolution of particles in aqueous or polar solutions. Mechanical mixing alone, either in molten or solidified paraffin, is also ineffective, because it results in poor uniformity of particle distribution. To overcome these disadvantages, we synthesized paraffin-compatible gold particles and developed an integration method wherein toluene is used as a phase transfer agent, and dodecanethiol to render particles strongly hydrophobic [74]. The nanoparticles were synthesized in toluene because of the

high solubility of paraffin in highly hydrophobic solvents. This approach enhanced the degree of homogeneous mixing of the nanoparticles in paraffin. This method allows integration of gold nanoparticles at room temperature, without the need for melting paraffin.

4.3.2 DSC Characterization

Thermal behavior of the pure paraffin and nanocompostite and also the influence of Au nanoparticles on the thermal properties of the pure paraffin wax have been characterized using DSC instrument (TA instruments Q1000, Newcastle, USA). Indium was used as a reference material to calibrate the system. The heating rate was 1 ˚C/min and heating temperature range was 20 ˚C to 70 ˚C. The samples of about 3.9 mg were crimped in an aluminum pan and placed inside the DSC cell. Samples of paraffin waxes were also weighed out and placed into the thermal analyses chamber. Via a computer and a separate thermal analysis processor these conditions were set: start at 20 ˚C, rate of heating 1 ˚C per minute, and final temperature of 70 ˚C. This process was repeated for all the samples.

The improvement of heat transfer was verified by comparing the nanocomposite and pure paraffin DSC thermograms in Figure 4.1. A DSC curve of paraffin was taken as a reference to evaluate the thermal changes of the nanocomposite. For pure paraffin wax there are two thermodynamic events, while there is only one endothermic peak for nanocomposite. The main endothermic peak in the thermograms represents the solid-liquid, or melting, transition of the

paraffin and nanocomposite, and the minor peak represents the transition of the paraffin wax from the crystalline phase into premelting phase. Paraffin is a mixture of different molecular sizes and crystalline components, which cause the paraffin to have two peaks. The melting point values were found to be 54 ± 1°C for paraffin, 42 ± 1°C for sample F, G and H. A 12 °C decrease in melting temperature is significant and supports the active role of the nanoparticles. As it is evident, nanoparticles of gold had dramatic impact on melting temperature of the paraffin wax. The broadening of melting point peaks may have been caused by gold impurities inside the nanocomposite.

Figure 4.1: DSC thermogram of the paraffin and nanocomposite.
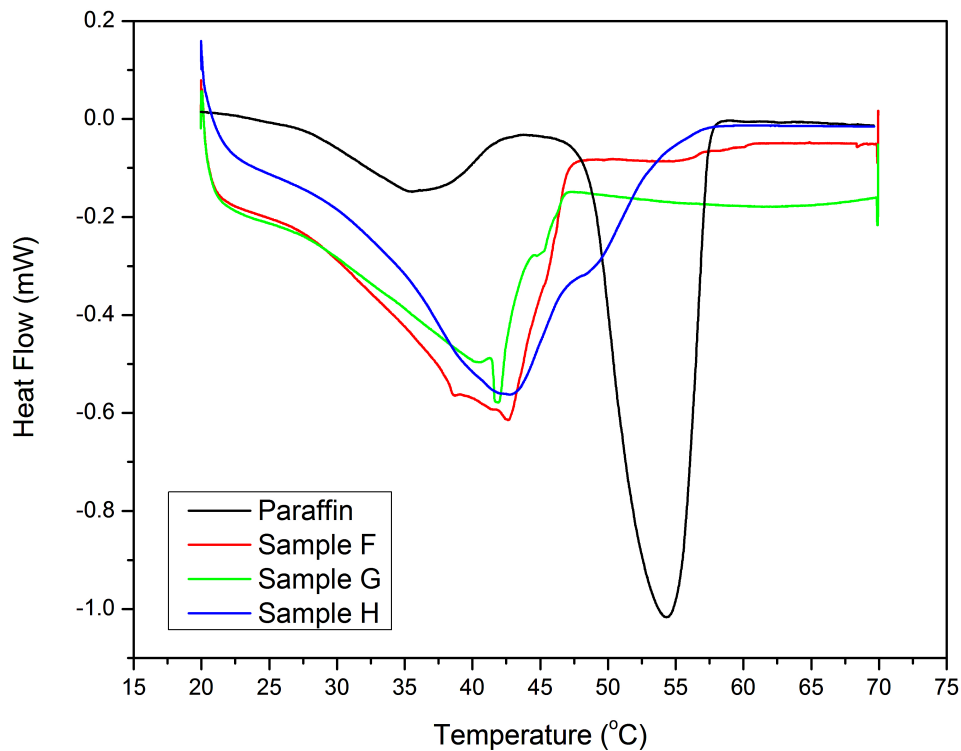
4.4 Results and Discussions

The morphology and dispersion uniformity of the nanoparticles were investigated through high resolution TEM microscopy (JEM-2200FS, JEOL Co., Ltd., Japan). Figure 4.2 shows TEM images of the nanoparticles of sample F, G and H in toluene.

(a)　　　　　　　　　　　　　　(b)

(c)
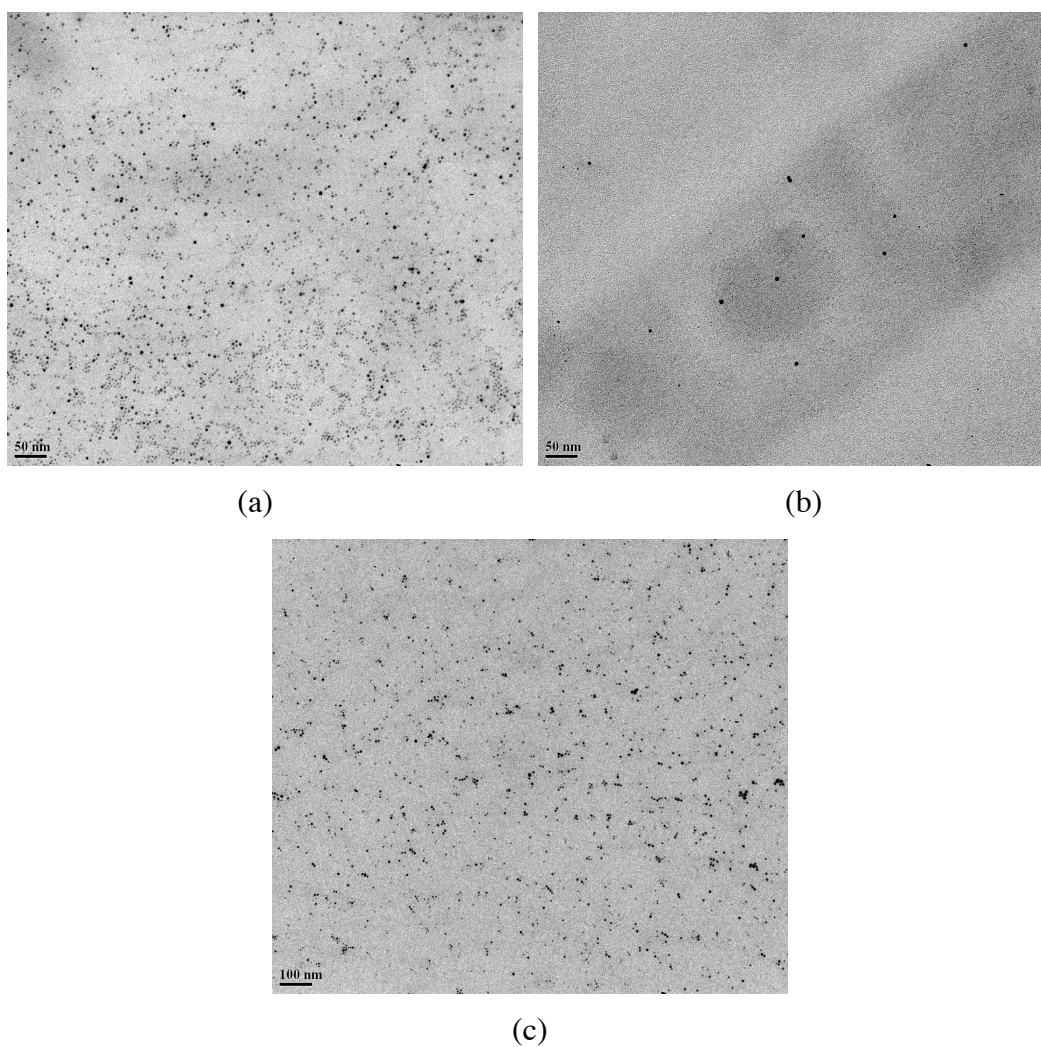
Figure 4.2: TEM micrograph of Au NPs for sample F (a), G (b) and H (c).

In another experiment nanoparticles were dispersed in the paraffin. To measure the particle size a small amount of the nanoparticle solution was placed onto a copper grid (carbon coated 400 mesh: TED Pella Inc., Redding, CA). The average particle size was 4 ± 2 nm.
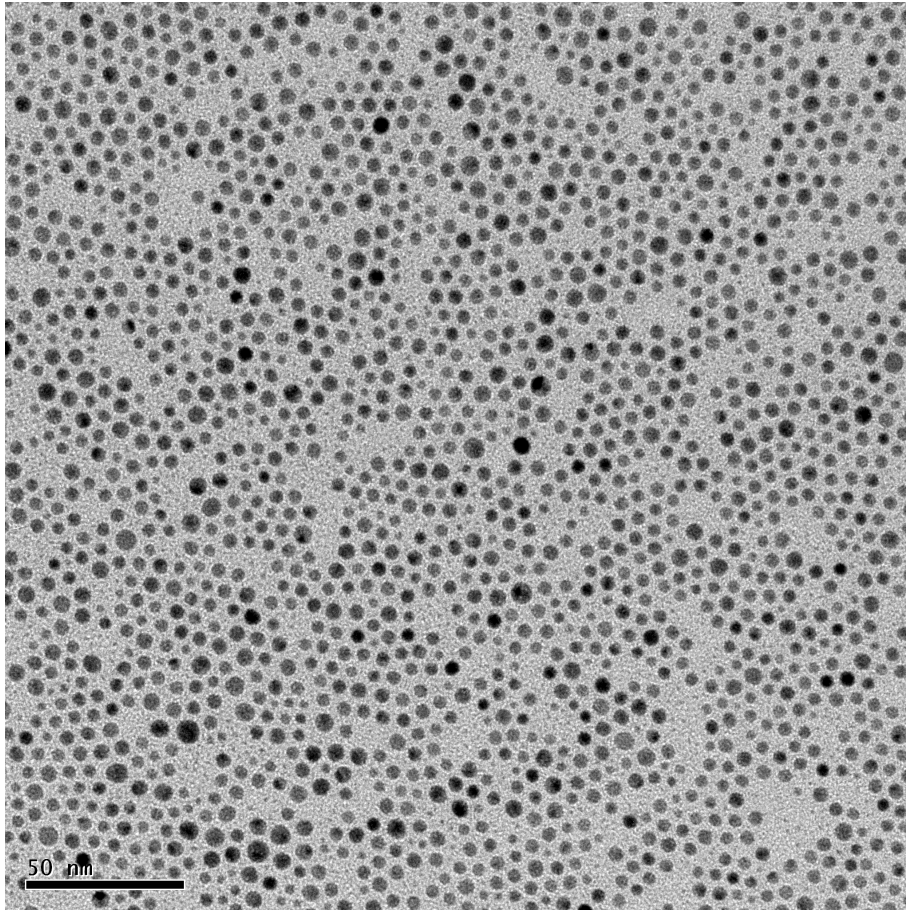
Figure 4.3: TEM microgra`gh of paraffin-AuNP composite showing uniform distribution of nanoparticles.

It was observed that nanoparticles were spherical and did not agglomerate when mixed with paraffin wax. They were dispersed uniformly and the size of the nanoparticles appeared to present a narrow distribution according to the TEM

images. This indicates that dodecanethiol surface modification of the nanoparticles effectively prevents agglomeration and leads to formation of well-dispersed nanoparticles. The spacing between the particles was about 2-4 nm. Images of the nanocomposite material is shown in Figure 4.3. After investigation of the nanoparticles using TEM, nanopaticles of sample F were found to be more homogenously dispersed.

Chapter 5

System Implementation

5.1 System Overview

The microactuator is made of photopolymer (SU-8) and consists of a reservoir sealed by a flexible membrane. The reservoir is self-filled with the nanocomposite material by capillarity. When heat is applied, the paraffin melts and generates pressure to deflect the membrane. A thermal actuation system was built in which the microactuator is placed on a Peltier cell and in contact with a heat sink. The Peltier is controlled with a LabVIEW program to inject or extract heat from the device.

5.2 Thermal Control system and Interfaces

A thermal system was built to actuate the membrane. A schematic of the system is depicted in Figure 5.1. The system was mainly comprised of a copper heatsink and a Peltier cell (Digi-key Corp., Thief River Falls, MN, US). A notch of 9×30 mm side length and 5 mm depth was machined in the heatsink and the Peltier was inserted and fastened with thermal epoxy. The chip with the microactuator was placed on the system and centered on the Peltier. A gap of ~300 μm is left

between the top of the Peltier and the chip to give room for a thin K-type thermocouple (Omega, Stamford, Connecticut). To connect the chip thermally to the Peltier, the gap was filled with silicone-based thermal paste.
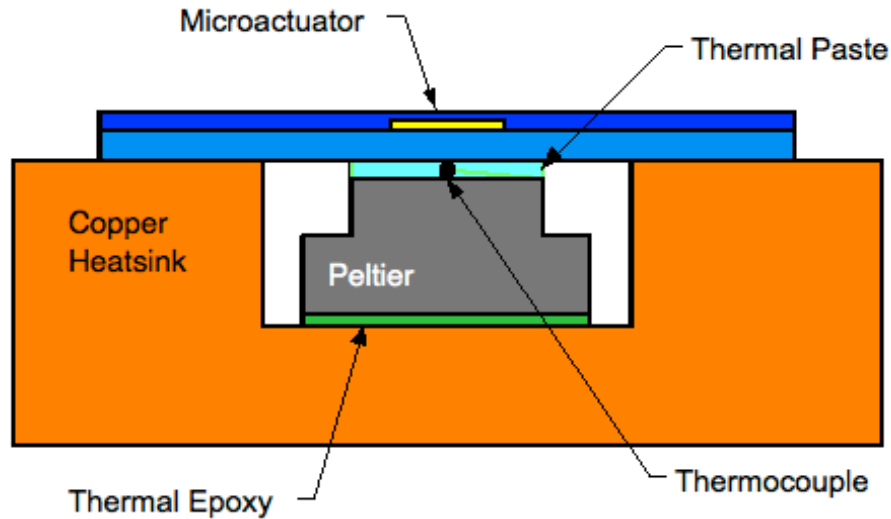
Figure 5.1: Schematic cross section of the thermal actuation system.

In this arrangement the heat generated by the Peltier flows from its top surface to the heatsink passing through the chip. The use of a heatsink allows efficient thermal control by providing a defined heat transfer path. Since the dominant heat loss mechanism is by conduction, heat loss due to convection becomes negligible, and hence fluctuations of ambient temperature produce minor perturbation to the system. In addition, the heatsink volume and surface are made large enough to keep its temperature unchanged from room temperature. Therefore, the heat flux through the chip is nearly constant after the initial transient. Due to the small thermal resistance path from the Peltier to the heatsink and the small mass of the chip, the heat flux establishes quickly, so the transient

time is minimized. The same occurs when the Peltier cools down under room temperature; just the heat flux through the chip is reversed. To control the system we developed a LabVIEW program, Figure 5.2, and an interface circuit, Figure 5.3.
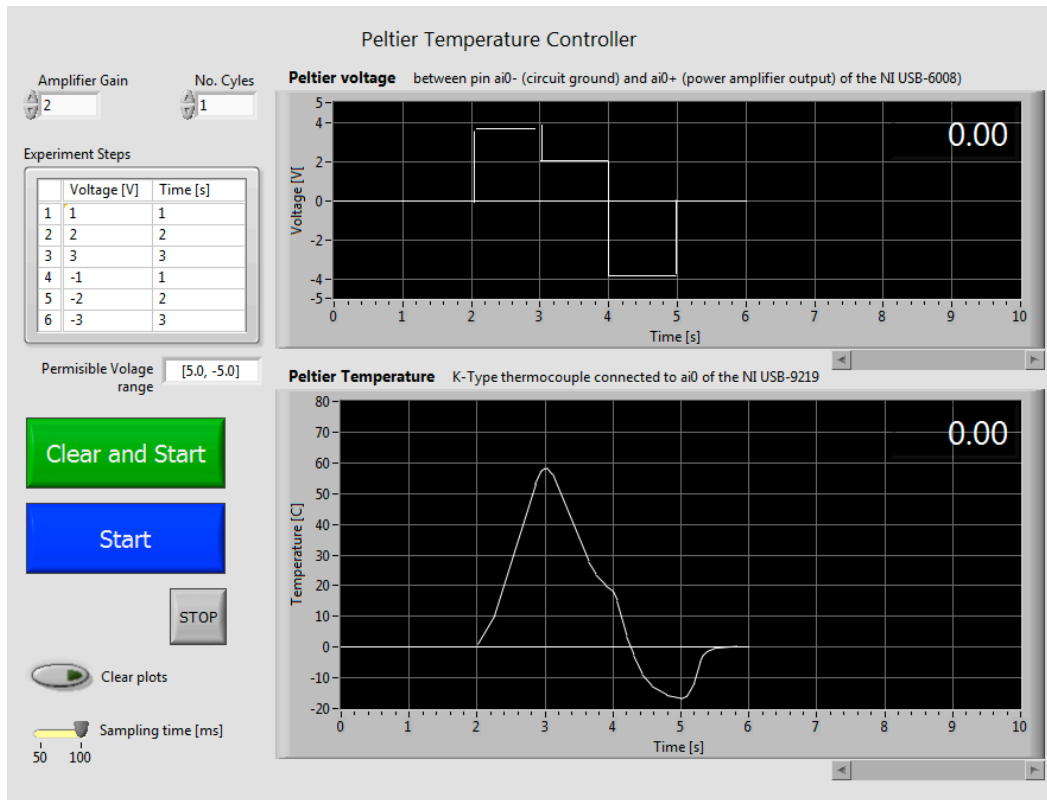
Figure 5.2: LabVIEW program for temperature control and monitoring. The top graph displays the voltage applied to the Peltier and the bottom graph displays the temperature at the bottom surface of the chip. The sequence of steps to execute is given in the list at the top left of the screen, specifying voltage and duration.

Note: the traces shown are just for program demonstration; the actual temperature trace of the experiments is shown in Figure 5.4.

54
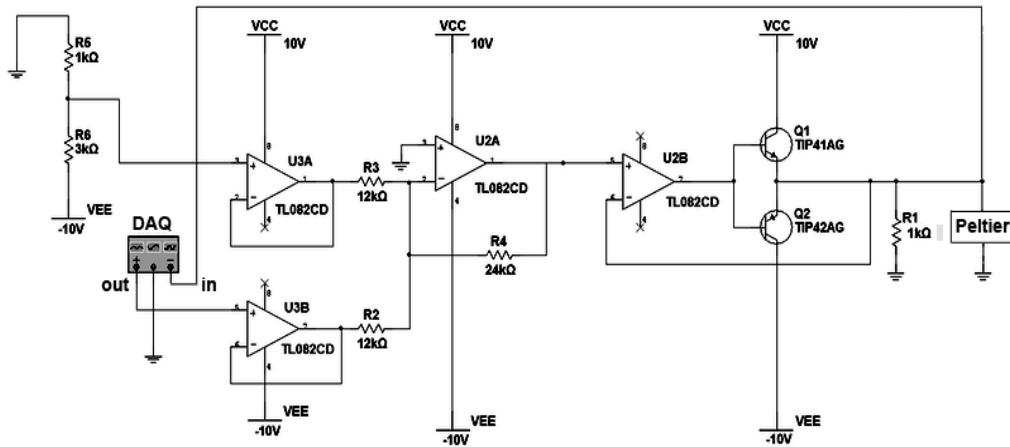
Figure 5.3: Schematic of the interface circuit. An analog-to-digital converter board connected to a computer that runs the LabVIEW control program provides a control signal that connects to the input buffer of the circuit (USB). The Peltier cell is connected to the emitter junction of the push-pull power amplifier.

The program monitors and records the temperature at the tip of the thermocouple through a data acquisition board (NI USB-9219, National Instruments). The program also generates a control signal for the Peltier, which is a sequence of voltage steps of duration and amplitude set by the user. The signal, which spans from 0 to 5 V is output by means of a data acquisition board (NI USB-6008, National Instruments) to the interface circuit. The circuit amplifies and offsets the signal to span from –5 V to +5 V, so the system can reverse the voltage of the Peltier to inject or extract heat from the chip. The last stage of the circuit is a power amplifier with voltage gain of 1 that directly drives the Peltier. The working voltage and current applied to the Peltier is within ±3.8 V and 1.5 A. The voltage across the terminals of the Peltier is acquired with the same board and plotted on screen.

55

For actuation experiments, we allowed the system to stabilize to room temperature and then started a sequence that produced a sharp temperature peak. The displacement of the membrane is simultaneously recorded employing a Doppler vibrometer. The maximum of the temperature peak is high enough to melt both the paraffin and the nanocomposite. The duration of the peak is made short, such that the membrane reaches only ~1/2 of its maximum deflection. The purpose of this is to avoid stressing the membrane beyond its elastic regime, because it may cause complete tearing or delamination from the bottom SU-8 layer.

5.3 Results and Discussion

5.3.1 Overall System Response

Five actuators filled with paraffin and five filled with the nanocomposite were subjected to a short temperature peak. The resulting displacement was then measured over time with a vibrometer. The typical response (Figure 5.4) shows that once melted, the paraffin and the nanocomposite expand at equal rates. However, the nanocomposite starts to expand after ~0.2 s, while pure paraffin has a lag of ~1s, approximately five times longer. The rising edge velocity for both is ~5.4 μm/s, while the falling edge velocity for paraffin is –2.5 μm/s and for the composite is –1.52 μm/s. The outcome is that the actuator with the nanocomposite reaches the rest position ~2 s before the one with paraffin. As a whole, the

paraffin completes the cycle in ~7.0 s and the nanocomposite in ~4.5 s. These results indicate that the nanocomposite effectively accepts or releases heat faster than pure paraffin, and this is a consequence of a reduction of the net thermal conductivity.
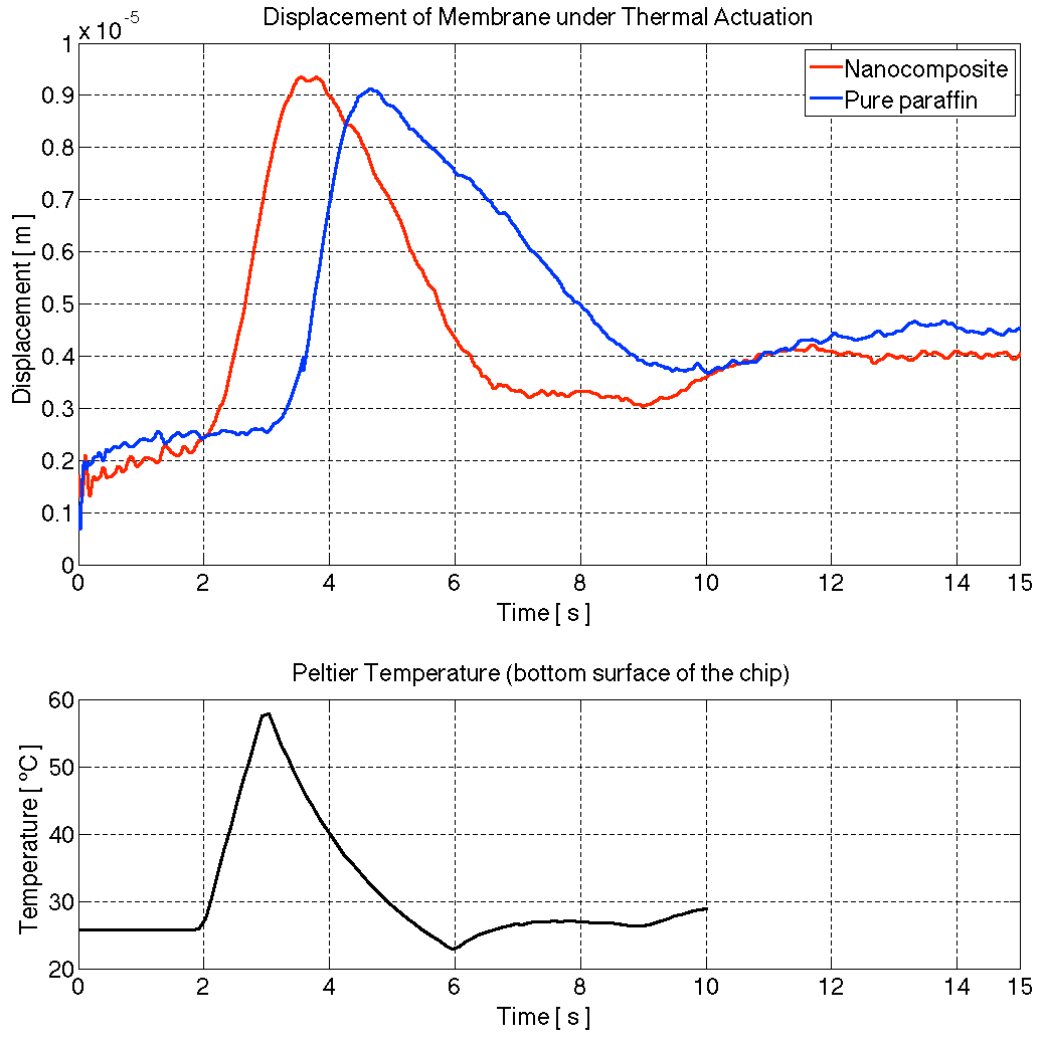

Figure 5.4: Dynamic response of the microactuator to a temperature peak, when filled with pure paraffin and when filled with the nanoparticle composite. The input step sequence is (voltage and time): 0V–2s, 3.8V–0.9s, -3V–3s, -0.5V–3s, 0V–inf. Note: our LabVIEW program only records 10s of data.

The total melting and solidification time of the actuator, filled with pure paraffin and with the nanocomposite, were measured by videotaping the process. The change in reflectivity of the paraffin and composite when solid or melted is easily detectable by optical means, as shown in Figure 5.5. The transit time between the fully solidified and fully melted states was measured to be approximately five times shorter for the nanocomposite. The maximum displacement of the membrane was 20 μm as measured with the vibrometer.

(a)   (b)
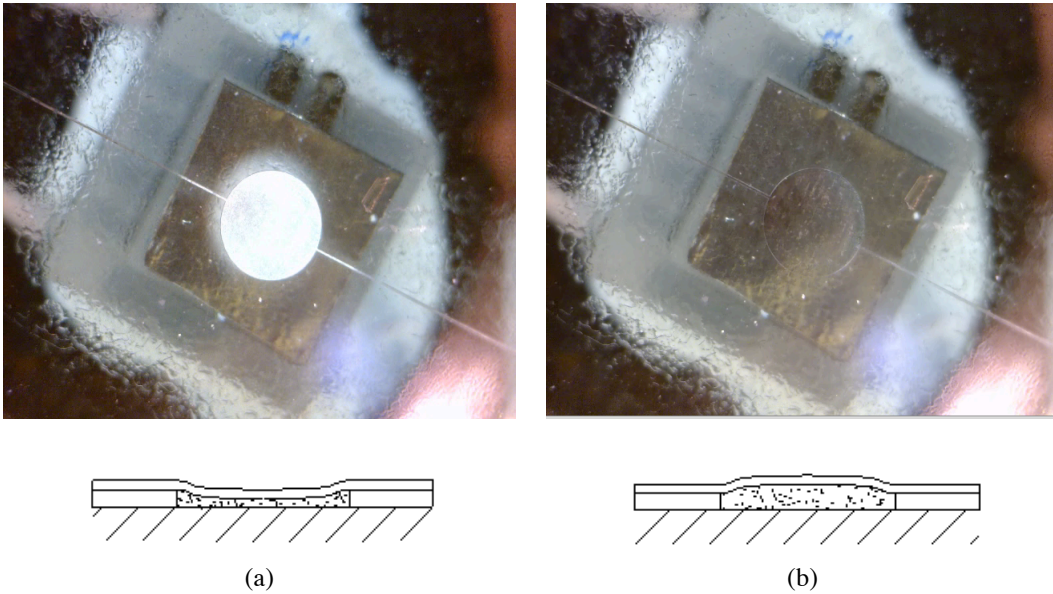
Figure 5.5: Top view of the microactuator, placed on the Peltier cell that thermally actuates the membrane. The actuator is in 1 mm radius and 50 μm thickness. The reservoir is self-filled with the nanocomposite by capillarity through access microchannels. (a) At temperatures under the melting point, the composite solidifies and pulls the membrane down to the recessed position. (b) At temperatures above the melting point, the composite melts and pushes the membrane up to the advanced position.

The membrane withstood the pressure in the reservoir without showing traces of tear or delamination. Despite the pressure generated, the molten paraffin did not flow out of the reservoir because the paraffin in the microchannels remained solid in most of their length. The reason is that the microchannels are in most of their length above the heatsink, thus they are nearly at 22 ˚C. In addition, the channels are very thin (100 x 40 μm) and long (>10 mm), hence they offer a very high resistance to flow. Taking advantage of the circular geometry of the actuator, we estimated the generated pressure from the governing equation for plate bending of the Classic Plate Theory, in polar coordinates [75], [76]:

$$\frac{\partial^4 w}{\partial r^4} + \frac{2}{r}\frac{\partial^3 w}{\partial r^3} - \frac{1}{r^2}\frac{\partial^2 w}{\partial r^2} + \frac{1}{r^3}\frac{\partial w}{\partial r} = \frac{p}{D} \qquad (1)$$

Where w is the displacement of the membrane as a function of the radial distance r; p is the applied pressure, and D is the flexural rigidity of the membrane, given by:

$$D = \frac{Eh^3}{12\left(1 - v^2\right)} \qquad (2)$$

Here h is the thickness of the membrane; E is the Young's modulus and v is Poisson's ratio of the material, which for SU-8 are around 3.2–4.4 GPa [77], [78] and 0.25 [78] respectively. For a clamped circular plate or membrane subjected to uniform pressure, (1) has a closed form solution [76], [79]:

59

$$w(r) = \frac{pa^4}{64D}\left[1 - \left(\frac{r}{a}\right)^2\right]^2 \qquad (3)$$

With a total radius of the membrane, the maximum deflection occurs at the center

point, where r = 0, thus (3) reduces to:

$$w_{max} = \frac{pa^4}{64D} \qquad (4)$$

The radius was 1 mm and the measured average maximum displacement at

the center was 10 μm from the flat position upwards. Solving (4) for p and

substituting values, where Emean =3.8 GPa and h = 10 μm, gives a pressure

generated by the composite of 216.88 Pa.

Chapter 6

Conclusion

6.1 Summary

We demonstrated a fast response polymer-based microactuator enabled by a novel phase change nanocomposite, which consists of gold nanoparticles tightly integrated to a paraffin vehicle. We also developed a novel recipe for the synthesis of paraffin-compatible gold nanoparticles, along with a method to integrate such particles in a paraffin matrix, creating intimate thermal contact with paraffin. The particles create a network of high thermal conductivity bridges in the paraffin. The particles also provide a large surface in contact with paraffin. These factors effectively facilitate heat flow through the material. The net effect of the enhanced thermal conductivity of the material manifests as a substantial reduction of its melting point, compared to pure paraffin, and hence the microactuator can use energy more efficiently and respond faster than with pure paraffin. Using these properties, we produced a microactuator with a total stroke of 20 μm in the vertical direction, 5.4 μm/s positive vertical displacement, 2.4 μm/s negative vertical displacement and <0.2 s lag time. The average size gold nanoparticles is ~4 nm and they are uniformly dispersed in paraffin, which implies that the new thermal properties of the composite are isotropic and

homogeneous. Gold is a biocompatible material and paraffin has very low chemical reactivity. Moreover, the composite is isolated from the environment by the membrane. Therefore, the microactuator can be used in contamination-sensitive applications, e.g. analysis of bio-molecules for medical diagnosis.

6.2 Future work

1. Microvalve

This design of microactuator can be used in microfluidic systems in order to control the fluid flow. A microvalve can be made by placing a discontinuous microchannel on top of a membrane. When the composite is solidified, the membrane is recessed and the fluid flows through the valve. When the composite is melted, the membrane moves upward and blocks flow. Figure 6.1 shows the top-view and cross-sectional view of the microchannels.
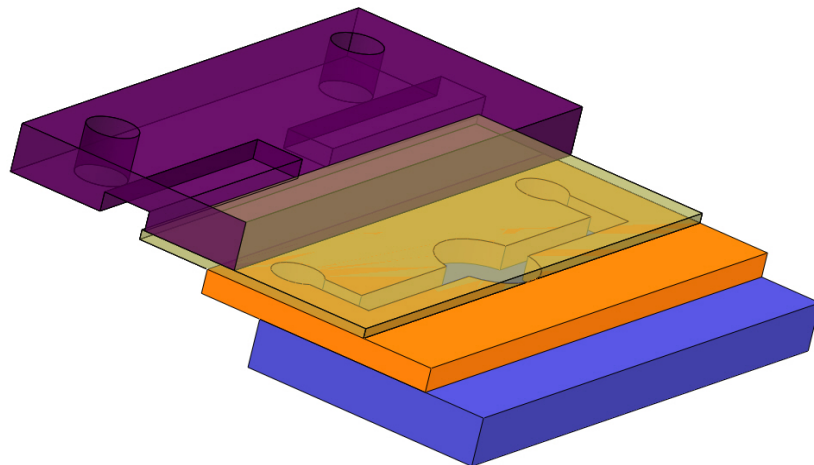
(a)
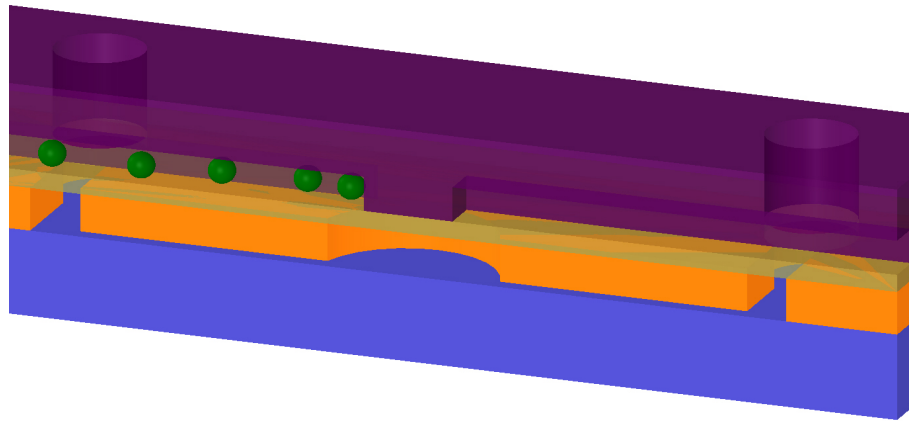
(b)
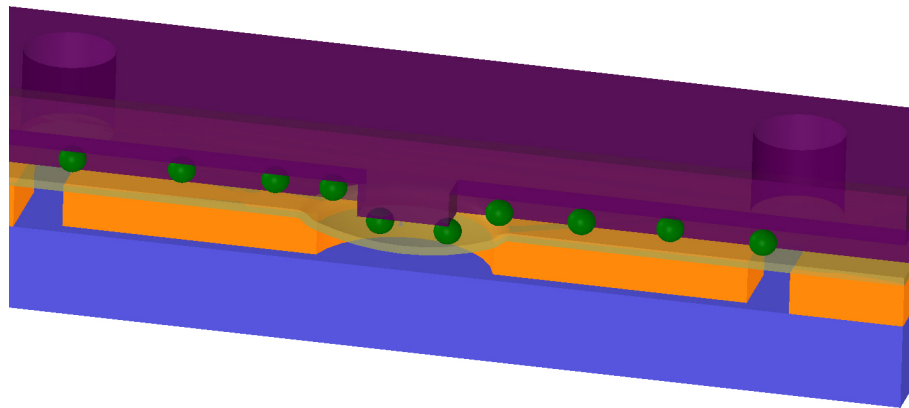
(c)

Figure 6.1: Cross-sectional view of the microvalve (a) three-layer microvlave (b) microvalve is closed (c) microvalve is open.

2. Temperature sensor

It can also be used as a temperature sensor (Figure 6.2) that can detect the temperature above the melting point in two ways. One way is as a variable capacitor and the other way is as a switch. It can be used as a thermostat to trigger a fan when the temperature is higher than a set point, in order to cool down the system.

Note: This switch can be made by patterning one of the electrodes/terminals on the membrane and the other one on an upper layer.

Figure 6.2: Cross-sectional view of a temperature sensor.

3. Microgrippers

Actuator can move the arms of the microgripper (Figure 6.3) against each other to handle a micro/nano-scale object.

Figure 6.3: Cross-sectional view of a microgripper.
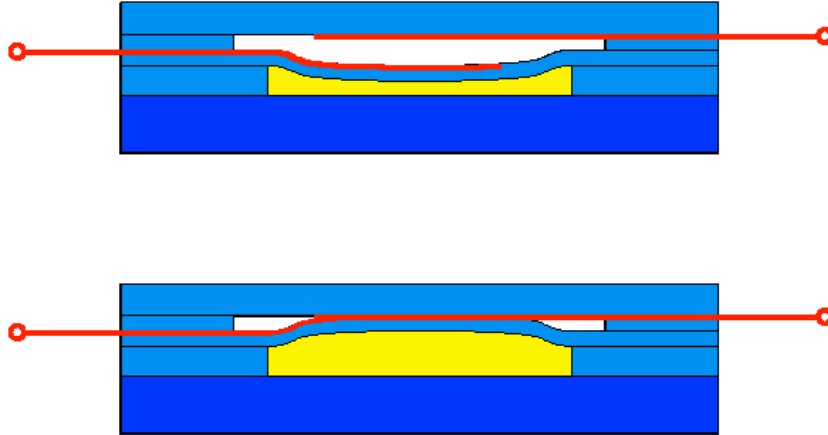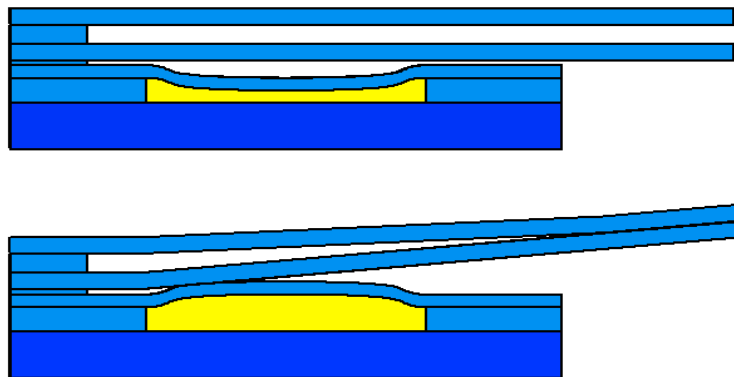
References

[1]   S. Cho, DK. Kang, J. Choo, A. J. de Mello, and SI. Chang, "Recent advances in microfluidic technologies for biochemistry and molecular biologys," *BMB Rep*, vol. 44, no. 11, pp. 705–712, Nov. 2011.

[2]   D. C. Duffy, J. C. McDonald, O. J. A. Schueller, and G. M. Whitesides, "Rapid Prototyping of Microfluidic Systems in Poly(dimethylsiloxane)," *Anal. Chem.*, vol. 70, no. 23, pp. 4974–4984, 1998.

[3]   A. Alrifaiy and K. Ramser, "How to integrate a micropipette into a closed microfluidic system: absorption spectra of an optically trapped erythrocyte," *Biomed Opt Express*, vol. 2, no. 8, pp. 2299–2306, Aug. 2011.

[4]   Y. Daghighi and D. Li, "Micro-valve using induced-charge electrokinetic motion of Janus particle," *Lab on a Chip*, vol. 11, no. 17, p. 2929, 2011.

[5]   A. Gaspar, M. Piyasena, L. Daroczi, and F. Gomez, "Magnetically controlled valve for flow manipulation in polymer microfluidic devices," *Microfluidics and Nanofluidics*, vol. 4, no. 6, pp. 525–531, 2008.

[6]   S. Shoji and M. Esashi, "Microflow devices and systems," *Journal of Micromechanics and Microengineering*, vol. 4, p. 157, 1994.

[7]   K. W. Oh and C. H. Ahn, "A review of microvalves," *J. Micromech. Microeng.*, vol. 16, no. 5, pp. R13–R39, Mar. 2006.

[8]   E. Thielicke and E. Obermeier, "Microactuators and their technologies," *Mechatronics*, vol. 10, no. 4, pp. 431–455, 2000.

[9]   T. Yasuda, I. Shimoyama, and H. Miura, "CMOS drivable electrostatic microactuator with large deflection," *Micro Electro Mechanical Systems, 1997. MEMS '97, Proceedings, IEEE, Tenth Annual International Workshop*, 1997, pp. 90 –95.

[10] C. R. Neagu, J. G. E. Gardeniers, M. Elwenspoek, and J. J. Kelly, "An electrochemical active valve," *Electrochimica Acta*, vol. 42, no. 20–22, pp. 3367–3373, 1997.

[11] R. G. Gilbertson and J. D. Busch, "A survey of micro-actuator technologies for future spacecraft missions," *Journal of the British Interplanetary Society*, vol. 49, no. 4, pp. 129–138, 1996.

[12] D. M. Kohl, *Shape Memory Microactuators*. Springer, 2004.

[13] M. De Volder and D. Reynaerts, "Pneumatic and hydraulic microactuators: a review," *Journal of Micromechanics and Microengineering*, vol. 20, no. 4, p. 043001, Apr. 2010.

[14] D. Anjewierden, G. A. Liddiard, and B. K. Gale, "An electrostatic microvalve for pneumatic control of microfluidic systems," *Journal of Micromechanics and Microengineering*, vol. 22, no. 2, p. 025019, Feb. 2012.

[15] W. H. Song, J. Kwan, G. V. Kaigala, V. N. Hoang, and C. J. Backhouse, "Readily integrated, electrically controlled microvalves," *Journal of Micromechanics and Microengineering*, vol. 18, no. 4, p. 045009, Apr. 2008.

[16] E. A. M. Graham, "Lab-on-a-Chip Technology," *FSMP*, vol. 1, no. 3, pp. 221–224, 2005.

[17] A. T. Giannitsis and M. Min, "Usage of microfluidic lab-on-chips in biomedicine," *Electronics Conference (BEC), 12th Biennial Baltic*, 2010, pp. 249–252.

[18] Y. Liu, C. B. Rauch, R. L. Stevens, R. Lenigk, J. Yang, D. B. Rhine, and P. Grodzinski, "DNA Amplification and Hybridization Assays in Integrated Plastic Monolithic Devices," *Anal. Chem.*, vol. 74, no. 13, pp. 3063–3070, Mar. 2012.

[19] D. J. Beebe, J. S. Moore, J. M. Bauer, Q. Yu, R. H. Liu, C. Devadoss, B. H. Jo, and others, "Functional hydrogel structures for autonomous flow control inside microfluidic channels," *Nature*, vol. 404, no. 6778, pp. 588–590, 2000.

[20] E. T. Carlen and C. H. Mastrangelo, "Surface micromachined paraffin-actuated microvalve," *Microelectromechanical Systems*, vol. 11, no. 5, pp. 408–420, 2002.

[21] L. Gui and J. Liu, "Ice valve for a mini/micro flow channel," *Journal of Micromechanics and Microengineering*, vol. 14, no. 2, pp. 242–246, Feb. 2004.

[22] A. K. Au, H. Lai, B. R. Utela, and A. Folch, "Microvalves and Micropumps for BioMEMS," *Micromachines*, vol. 2, no. 2, pp. 179–220, May 2011.

[23] L. Gui, B. Y. Yu, C. L. Ren, and J. P. Huissoon, "Microfluidic phase change valve with a two-level cooling/heating system," *Microfluid Nanofluid*, vol. 10, no. 2, pp. 435–445, Aug. 2010.

[24] R. Pal, M. Yang, B. N. Johnson, D. T. Burke, and M. A. Burns, "Phase Change Microvalve for Integrated Devices," *Anal. Chem.*, vol. 76, no. 13, pp. 3740–3748, Feb. 2012.

[25] Bozhi Yang and Qiao Lin, "A Latchable Phase-Change Microvalve With Integrated Heaters," *Microelectromechanical Systems*, vol. 18, no. 4, pp. 860–867, 2009.

[26] P. Selvaganapathy, E. . Carlen, and C. . Mastrangelo, "Electrothermally actuated inline microfluidic valve," *Sensors and Actuators A: Physical*, vol. 104, no. 3, pp. 275–282, May 2003.

[27] S. M. Hasnain, "Review on sustainable thermal energy storage technologies, Part I: heat storage materials and techniques," *Energy Conversion and Management*, vol. 39, no. 11, pp. 1127–1138, 1998.

[28] A. Karaipekli and Sari, "Thermal conductivity and latent heat thermal energy storage characteristics of paraffin/expanded graphite composite as phase change material," *Applied Thermal Engineering*, vol. 27, no. 8–9, pp. 1271–1277, 2007.

[29] J. W. Judy, "Microelectromechanical systems (MEMS): fabrication, design and applications," *Smart Materials and Structures*, vol. 10, no. 6, pp. 1115–1134, Dec. 2001.

[30] H. Helvajian, *Microengineering Aerospace Systems*. AIAA, 1999.

[31] G. Coppola, P. Ferraro, M. Iodice, S. De Nicola, A. Finizio, and S. Grilli, "MEMS inspection by Digital Holographic," *Microelectronics, 2004. 24th International Conference on*, 2004, vol. 1, pp. 213 – 216 vol.1.

[32] H. Fujita, "A decade of MEMS and its future," *Micro Electro Mechanical Systems, 1997. MEMS '97, Proceedings, IEEE., Tenth Annual International Workshop on*, 1997, pp. 1 –7.

[33] D. Logan, "Defect-enhanced Silicon Photodiodes for Photonic Integrated Circuits," *Open Access Dissertations and Theses*, Oct. 2011.

[34] M. Mehregany, "Microelectromechanical systems," *Circuits and Devices Magazine, IEEE*, vol. 9, no. 4, pp. 14 –22, Jul. 1993.

[35] M. J. Madou, *Fundamentals of Microfabrication: The Science of Miniaturization, Second Edition*, 2nd ed. CRC Press, 2002.

[36] N. S. K. Hasikin, "Modeling of a polyimide diaphragm for an optical pulse pressure sensor," pp. 1 – 5, 2010.

[37] H. A. Stone and S. Kim, "Microfluidics: Basic issues, applications, and challenges," *AIChE Journal*, vol. 47, no. 6, pp. 1250–1254, 2001.

[38] J. Manuel, "Fluid Movement," *Environ Health Perspect*, vol. 114, no. 12, pp. A710–A713, Dec. 2006.

[39] H. Becker and L. E. Locascio, "Polymer microfluidic devices," *Talanta*, vol. 56, no. 2, pp. 267–287, Feb. 2002.

[40] J. Kameoka, H. G. Craighead, H. Zhang, and J. Henion, "A Polymeric Microfluidic Chip for CE/MS Determination of Small Molecules," *Anal. Chem.*, vol. 73, no. 9, pp. 1935–1941, 2001.

[41] P. Belgrader, M. Okuzumi, F. Pourahmadi, D. A. Borkholder, and M. A. Northrup, "A microfluidic cartridge to prepare spores for PCR analysis," *Biosensors and Bioelectronics*, vol. 14, no. 10–11, pp. 849–852, Jan. 2000.

[42] E. T. Lagally, I. Medintz, and R. A. Mathies, "Single-Molecule DNA Amplification and Analysis in an Integrated Microfluidic Device," *Anal. Chem.*, vol. 73, no. 3, pp. 565–570, 2001.

[43] J. Khandurina, T. E. McKnight, S. C. Jacobson, L. C. Waters, R. S. Foote, and J. M. Ramsey, "Integrated System for Rapid PCR-Based DNA Analysis in Microfluidic Devices," *Anal. Chem.*, vol. 72, no. 13, pp. 2995–3000, 2000.

[44] B. A. Buchholz, E. A. S. Doherty, M. N. Albarghouthi, F. M. Bogdan, J. M. Zahn, and A. E. Barron, "Microchannel DNA Sequencing Matrices with a Thermally Controlled 'Viscosity Switch'," *Anal. Chem.*, vol. 73, no. 2, pp. 157–164, 2000.

[45] Z. H. Fan, S. Mangru, R. Granzow, P. Heaney, W. Ho, Q. Dong, and R. Kumar, "Dynamic DNA hybridization on a chip using paramagnetic beads," *Anal. Chem.*, vol. 71, no. 21, pp. 4851–4859, Nov. 1999.

[46] L. Koutny, D. Schmalzing, O. Salas-Solano, S. El-Difrawy, A. Adourian, S. Buonocore, K. Abbey, P. McEwan, P. Matsudaira, and D. Ehrlich, "Eight Hundred-Base Sequencing in a Microfabricated Electrophoretic Device," *Anal. Chem.*, vol. 72, no. 14, pp. 3388–3391, 2000.

[47] GB. Lee, SH. Chen, GR. Huang, WC. Sung, and YH. Lin, "Microfabricated plastic chips by hot embossing methods and their applications for DNA separation and detection," *Sensors and Actuators B: Chemical*, vol. 75, no. 1–2, pp. 142–148, Apr. 2001.

[48] J. Yang, Y. Huang, XB. Wang, F. F. Becker, and P. R. C. Gascoyne, "Cell Separation on Microfabricated Electrodes Using Dielectrophoretic/Gravitational Field-Flow Fractionation," *Anal. Chem.*, vol. 71, no. 5, pp. 911–918, 1999.

[49] A. Coraci, C. Podaru, E. Manea, A. Ciuciumis, and O. Corici, "New technological surface microfabrication methods used to obtain microchannels based systems onto various substrates," *Semiconductor Conference, 2005. CAS 2005 Proceedings. 2005 International*, 2005, vol. 1, pp. 249 – 252 vol. 1.

[50] L. Bousse, C. Cohen, T. Nikiforov, A. Chow, A. R. Kopf-Sill, R. Dubrow, and J. W. Parce, "Electrokinetically Controlled Microfluidic Analysis

Systems," *Annual Review of Biophysics and Biomolecular Structure*, vol. 29, no. 1, pp. 155–181, 2000.

[51] D. R. Reyes, D. Iossifidis, PA. Auroux, and A. Manz, "Micro Total Analysis Systems. 1. Introduction, Theory, and Technology," *Anal. Chem.*, vol. 74, no. 12, pp. 2623–2636, Jun. 2002.

[52] J. C. Kurnia, E. Birgersson, and A. S. Mujumdar, "Computational Study of pH-sensitive Hydrogel-based Microfluidic Flow Controllers," *Journal of Functional Biomaterials*, vol. 2, no. 3, pp. 195–212, Aug. 2011.

[53] NT. Nguyen and S. T. Wereley, *Fundamentals and Applications of Microfluidics*. Artech House, 2002.

[54] W. K. Schomburg, *Introduction to Microsystem Design*. Springer, 2011.

[55] D. Xing, Y. Li, and C. Zhang, "Micropumps, microvalves, and micromixers within PCR microfluidic chips: Advances and trends.," *Biotechnology Advances*, vol. 25, no. 5, pp. 483–514, 2007.

[56] KK. Liu, RG. Wu, YJ. Chuang, H. S. Khoo, SH. Huang, and FG. Tseng, "Microfluidic Systems for Biosensing," *Sensors*, vol. 10, no. 7, pp. 6623–6661, May 2010.

[57] B. Bhushan, *Springer Handbook of Nanotechnology*. Springer, 2006.

[58] WM. Zhang, G. Meng, and D. Chen, "Stability, Nonlinearity and Reliability of Electrostatically Actuated MEMS Devices," *Sensors*, vol. 7, no. 5, pp. 760–796, May 2007.

[59] M. P. Chang and M. M. Maharbiz, "Electrostatically-actuated reconfigurable elastomer microfluidics," in *Proc. 13th Solid-State Sensor, Actuator, and Microsystems Workshop (Hilton Head'08)*, 2008, pp. 122–125.

[60] TR. Hsu, *Mems and Microsystems: Design, Manufacture, and Nanoscale Engineering*. John Wiley & Sons, 2008.

[61] T. Watanabe and H. Kuwano, "A microvalve matrix using piezoelectric actuators," *Microsystem Technologies*, vol. 3, no. 3, pp. 107–111, May 1997.

[62] D. J. Bell, T. J. Lu, N. A. Fleck, and S. M. Spearing, "MEMS actuators and sensors: observations on their performance and selection for purpose," *Journal of Micromechanics and Microengineering*, vol. 15, p. S153, 2005.

[63] Z. R. T. Rogge, "Polymer micro valve with a hydraulic piezo-drive fabricated by the AMANDA process," *Sensors and Actuators A: Physical*, pp. 206–212.

[64] L. Klintberg, "A large stroke, high force paraffin phase transition actuator," *Sensors and actuators. A Physical*, vol. 96, p. 189, Feb. 2002.

[65] E. T. Carlen and C. H. Mastrangelo, "Electrothermally activated paraffin microactuators," *Microelectromechanical Systems, Journal of*, vol. 11, no. 3, pp. 165–174, 2002.

[66] F. Goldschmidtboing, P. Katus, A. Geipel, and P. Woias, "A novel self-heating paraffin membrane micro-actuator," *Micro Electro Mechanical Systems, 2008. MEMS 2008. IEEE 21st International Conference*, 2008, pp. 531–534.

[67] D. R. Lide, *CRC Handbook of Chemistry and Physics*, 90th ed. CRC Press, 2009.

[68] JM. Park, YK. Cho, BS. Lee, JG. Lee, and C. Ko, "Multifunctional microvalves control by optical illumination on nanoheaters and its application in centrifugal microfluidic devices," *Lab on a Chip*, vol. 7, no. 5, pp. 557–564, 2007.

[69] M. De Voider, F. Ceyssens, D. Reynaerts, and R. Puers, "Microsized Piston-Cylinder Pneumatic and Hydraulic Actuators Fabricated by Lithography," *Microelectromechanical Systems*, vol. 18, no. 5, pp. 1100 –1104, Oct. 2009.

[70] T. Ohori, S. Shoji, K. Miura, and A. Yotsumoto, "Partly disposable three-way microvalve for a medical micro total analysis system (μTAS)," *Sensors and Actuators A: Physical*, vol. 64, no. 1, pp. 57–62, Jan. 1998.

[71] K. Hosokawa and R. Maeda, "A pneumatically-actuated three-way microvalve fabricated with polydimethylsiloxane using the membrane

transfer technique," *Journal of micromechanics and microengineering*, vol. 10, p. 415, 2000.

[72] F. E. H. Tay, J. A. van Kan, F. Watt, and W. O. Choong, "A novel micro-machining method for the fabrication of thick-film SU-8 embedded micro-channels," *J. Micromech. Microeng.*, vol. 11, no. 1, pp. 27–32, Jan. 2001.

[73] W. Chen, R. H. W. Lam, and J. Fu, "Photolithographic surface micromachining of polydimethylsiloxane (PDMS)," *Lab on a Chip*, vol. 12, no. 2, p. 391, 2012.

[74] A. Kyrychenko, "Preparation, structure, and a coarse-grained molecular dynamics model for dodecanethiol-stabilized gold nanoparticles," *Computational and Theoretical Chemistry*, vol. 977, no. 1–3, pp. 34–39, 2011.

[75] P. G. Lowe, *Basic principles of plate theory*. Surrey University Press, 1982.

[76] A. Ugural, *Stresses in plates and shells*, 2nd ed. Boston: WCB/McGraw Hill, 1999.

[77] T. Chu Duc, "Polymeric Thermal Microactuator With Embedded Silicon Skeleton: Part II -- Fabrication, Characterization, and Application for 2-DOF Microgripper," *Ieeeasme Journal Of Microelectromechanical Systems*, vol. 17, no. 4, p. 823, Jan. 2008.

[78] NT. Nguyen, SS. Ho, and C. LN. Low, "A polymeric microgripper with integrated thermal actuators," *Journal of Micromechanics and Microengineering*, vol. 14, no. 7, pp. 969–974, Jul. 2004.

[79] J. A. Voorthuyzen, A. J. Sprenkels, A. G. H. Van Der Donk, P. R. Scheeper, and P. Bergveld, "Optimization of capacive microphone and pressure sensor performance by capacitor-electrode shaping," *Sensors and Actuators A: Physical*, vol. 26, no. 1–3, pp. 331–336, Mar. 1991.